LBNL-47231

ERNEST ORLANDO LAWRENCE
BERKELEY NATIONAL LABORATORY

Chemical Reaction Dynamics Using Semiclassical Methods

Kathy Lynne Sorge

Chemical Sciences Division

December 2000

Ph.D. Thesis

REFERENCE COPY
Does Not
Circulate

Lawrence Berkeley National Laboratory

Annex

Copy 1

LBNL-47231

DISCLAIMER

This document was prepared as an account of work sponsored by the United States Government. While this document is believed to contain correct information, neither the United States Government nor any agency thereof, nor the Regents of the University of California, nor any of their employees, makes any warranty, express or implied, or assumes any legal responsibility for the accuracy, completeness, or usefulness of any information, apparatus, product, or process disclosed, or represents that its use would not infringe privately owned rights. Reference herein to any specific commercial product, process, or service by its trade name, trademark, manufacturer, or otherwise, does not necessarily constitute or imply its endorsement, recommendation, or favoring by the United States Government or any agency thereof, or the Regents of the University of California. The views and opinions of authors expressed herein do not necessarily state or reflect those of the United States Government or any agency thereof or the Regents of the University of California.

LBNL-47231

Chemical Reaction Dynamics using Semiclassical Methods

Kathy Lynne Sorge
Ph.D. Thesis

Department of Chemistry
University of California, Berkeley

and

Chemical Sciences Division
Ernest Orlando Lawrence Berkeley National Laboratory
University of California
Berkeley, CA 94720

December 2000

This work was supported by the Director, Office of Science, Office of Basic Energy Sciences, Chemical Sciences Division of the U.S. Department of Energy under Contract No. DE-AC03 76SF00098, Lawrence Berkeley National Laboratory, and also by the National Science Foundation under Grant No. CHE97-32758.

Chemical Reaction Dynamics using Semiclassical Methods

by

Kathy Lynne Sorge

B. S. (University of California, Los Angeles) 1995

A dissertation submitted in partial satisfaction of the
requirements for the degree of
Doctor of Philosophy
in
Chemistry
in the
GRADUATE DIVISION
of the
UNIVERSITY of CALIFORNIA, BERKELEY

Committee in Charge:
Professor William H. Miller, Chair
Professor Martin Head-Gordon
Professor Robert G. Littlejohn

Fall 2000

Chemical Reaction Dynamics using Semiclassical Methods

Copyright ©2000

by

Kathy Lynne Sorge

The U.S. Department of Energy has the right to use this document
for any purpose whatsoever including the right to reproduce
all or any part thereof.

Abstract

Chemical Reaction Dynamics using Semiclassical Methods

by
Kathy Lynne Sorge

Doctor of Philosophy in Chemistry
University of California, Berkeley
Professor William H. Miller, Chair

This work presents several semiclassical techniques for calculating properties of chemical systems. We would ideally like to perform all calculations in a fully quantum mechanical manner. However, as the dimensions of the system of interest increase, so does the computational complexity of the quantum calculations. At some point the quantum calculations become intractable, and we must derive and use approximate methods. Semiclassical mechanics provides a way to estimate or approximate these quantum effects. In this work, we examine three such semiclassical techniques and variations of those methods.

First we look at Semiclassical Transition State Theory(SCTST), which uses a semiclassical approximation for tunneling through a reaction barrier. We note that the semiclassical tunneling probability can be replaced by the quantum tunneling probability for the Eckart barrier. When we apply these two methods to the $H_2 + OH \rightarrow H_2O + H$, $D_2 + OH \rightarrow HDO + D$, and $Cl + H_2 \rightarrow HCl + H$ reactions, we find that SCTST results agree closely with previous experimental and quantum results. The results for reactions without hydrogen motion are especially accurate.

Next we use the Semiclassical Perturbation (SCP) and Infinite Order Sudden (IOS) approximations to calculate the dissociation rate of triplet ketene. Previous experiments have shown a definite step structure in the rate when the total energy of the system is increased. For our calculations, we use a newly available potential energy surface that is calculated at a high level of theory. Unfortunately, we were unable to reproduce the step structure and elucidate the underlying principles behind the steps. However, we do see structure in the rate as the curvature couplings are artificially increased.

Lastly, we explore the nuances of the Herman-Kluk Initial Value Representation (IVR), where the propagator is expressed as a phase space average. We apply this method to a model system, where we can control the chaotic nature of the system. As the chaotic nature of the system is increased, the Monte Carlo evaluation of the phase space integral becomes difficult to converge. In an attempt to smooth the integrand, we introduce a time average in the Herman-Kluk formalism. This new method in effect adds a zero point energy to the classical hamiltonian. For the less chaotic systems, this new method does result in a severe decrease in the number of trajectories necessary for convergence. However, the splittings in the spectrum are underestimated at higher couplings.

To everyone who has and continues to support me.
Thank you.

Contents

Table of Contents iii

List of Figures v

List of Tables vii

1 Introduction 1

2 Semiclassical Transition State Theory 5
- 2.1 Introduction . . . 5
  - 2.1.1 The Rate Equation . . . 7
- 2.2 Semiclassical Transition State Theory . . . 8
- 2.3 SCTST/QM . . . 12
- 2.4 $H_2 + OH \rightarrow H_2O + H$ . . . 13
  - 2.4.1 Computational Specifics . . . 13
  - 2.4.2 Results . . . 15
- 2.5 $Cl + H_2 \rightarrow HCl + H$ . . . 16
  - 2.5.1 Computational Specifics . . . 16
  - 2.5.2 Results . . . 21
- 2.6 Conclusions . . . 23

3 Dissociation of Triplet Ketene 24
- 3.1 Introduction . . . 24
- 3.2 Potential Energy Surface . . . 26
- 3.3 Theoretical Methods . . . 31
  - 3.3.1 DVR-ABC . . . 31
  - 3.3.2 SCP-IOS . . . 33
  - 3.3.3 J-Shifting . . . 35
- 3.4 Results . . . 36
- 3.5 Conclusions . . . 40

4 Time Averaging the SCIVR **42**
4.1 Introduction 42
4.2 The SCIVR Formalism 43
4.3 Time Averaging 45
4.4 Computational Specifics 48
4.4.1 Hamiltonian 48
4.4.2 The Wave Function and Overlaps 48
4.4.3 HK-SCIVR 49
4.4.4 Time Averaging 51
4.5 Results 53
4.6 Conclusions 60

5 Summary and Conclusions **61**
5.1 Summary 61
5.2 The Future of IVR Methods 63
5.3 Conclusions 64

References **65**

List of Figures

2.1 Thermal Rate for $H_2 + OH \rightarrow H_2O + H$,J=0 17
2.2 Thermal Rate for $H_2 + OH \rightarrow H_2O + H$ 18
2.3 Thermal Rate for $D_2 + OH \rightarrow HDO + H$,J=0 19
2.4 Thermal Rate for $D_2 + OH \rightarrow HDO + H$ 20
2.5 Thermal Rate for $Cl + H_2 \rightarrow HCl + H$ 22

3.1 C_s^{II} Transition State of Triplet Ketene 29
3.2 1D Potential Surface for Triplet Ketene 30
3.3 1D Cumulative Reaction Probability 37
3.4 Dissociation Rate for Triplet Ketene 38
3.5 Dissociation Rates for Increased Couplings 39

4.1 Model Potential Energy Surface 50
4.2 The Phase of the Pre-exponential Factor 52
4.3 Spectrum of a Model Hamiltonian 56
4.4 Spectrum of a Model Hamiltonian 57
4.5 Spectrum of a Model Hamiltonian 58
4.6 Spectrum of a Model Hamiltonian 59

List of Tables

3.1 Parameters for Reactant Partition Function 27
3.2 Potential Energy of Triplet Ketene 28
3.3 Parameters for the Absorbing Potentials 33
3.4 Rotational Constants for Triplet Ketene 36

4.1 Percent of Trajectories with Imaginary Local Frequencies 55

Acknowledgements

First and foremost, I would like to thank Prof. Miller for taking me into his research group. He has provided invaluable insight and support in my quest for knowledge. It has been my pleasure to learn from and interact with such an exceptional chemist. I have also learned a tremendous amount in the process of serving as a teaching assistant in Prof. Miller's kinetics class. I'm not sure who learned more, the students or me.

I would also like to thank Cheryn Gliebe for all of her support and friendship. She always knows who to call and where to get everything. Her efforts to keep the group running smoothly are greatly appreciated.

Many thanks go out to the whole Miller group, past and present. It has been a joy to work and interact with people with such different backgrounds. These backgrounds have provided an interesting view into many cultures and many varied approaches to theoretical chemistry. I would like to acknowledge Dr. Victor Batista, Dr. Eduardo Coronado, Steve Cotton, Dr. Tim Germann, Prof. Dan Gezelter, Dr. Victor Guallar, Prof. Xavier Gimenez, Dr. Stephan Krempl, Dr. Frank Matzkies, Dr. Bill Poirier, Bruce Spath, Dr. Sean Sun, Prof. Ward Thompson, Dr. Clemens Woywod, and Jianhua Xing.

I would particularly like to thank the Miller group members with whom I have had the opportunity to work closely: Dr. David Skinner and Dr. Haobin Wang. David proved to be a wonderful teacher of chemistry and all things computer related. Through David I learned more about Unix and fixing computer problems myself, or at least investigating them. Haobin has also been an invaluable and patient teacher. He has a tremendous amount of experience and knowledge about many different theoretical methods. I have enjoyed working closely with both David and Haobin.

Many thanks go to the wonderful professors who taught the classes that I had the opportunity to take. I have often referred back to my notes from all my classes, and they maintain a prominent position on my bookshelves. Thank you specifically to Prof. Harris, Prof. Head-Gordon, Prof. Lester, Prof. Littlejohn,

and Prof. Miller. I enjoyed all of your classes immensely.

I'd like to thank Prof. Emily Carter. I had the extreme pleasure of studying with her as an undergraduate. Her gentle prodding and ceaseless encouragement helped to pave my path to graduate school.

Lastly, a big thank you to all my friends and family who have supported me throughout my graduate career. Thanks to Matt for helping me learn about jobs in the real world, Ian for providing a floor to sleep on, Dave for his movie collection, Maria for applied chemistry lessons in winemaking, and Josh for his videogame expertise. Finally, special thanks go out to my family and fiancé, Mike. I would not be where I am today without all of your encouragement and support.

This work has been supported by the Director, Office of Science, Office of Basic Energy Sciences, Chemical Sciences Division of the U.S. Department of Energy under contract No. DE-AC03 76SF00098, Lawrence Berkeley National Laboratory, and also by the National Science Foundation under Grant No. CHE97-32758.

Chapter 1

Introduction

In chemistry, we are interested in both how molecules behave alone and how they interact with each other. Theoretical chemists try to elucidate the underlying processes of chemical systems by means of equations and calculations, while the experimentalists play with the chemical systems in a similar attempt. Together we try to *crack* the code as to why matter behaves as it does, thereby obtaining a complete understanding of the full reaction. A detailed understanding of the reaction has many applications, from being able to control the reaction more precisely to predicting the interaction of other molecules.

As theorists, our most accurate, fully exact method is quantum mechanics. While a large object (such as a baseball) obeys classical mechanical principles, the motions of light objects (such as atoms) are governed by quantum mechanics. Quantum mechanics allows for a variety of phenomena not seen in classical mechanics. These include coherence and tunneling, which can contribute significantly to the physical properties of interest.

In quantum mechanics, all physical properties of a chemical system can be obtained from the wave function. However, the wave function can be very difficult to obtain because most quantum methods rely on the use of basis sets. If we use N basis sets for each degree of freedom, we see how the number of basis

sets required for a large dimensional system can quickly become unwieldy. The number of basis functions necessary for an accurate calculation increases exponentially with the number of degrees of freedom. Although we would ideally like to perform all calculations quantum mechanically and thus exactly, this is often not possible using today's technology. Many chemical systems of interest are too large to treat using quantum mechanics due to memory constraints. In fact it was only a few year ago that the first four-dimensional calculations were performed.

At some point we must ask ourselves if each system needs to be treated using quantum mechanics. While it is true that isolated reactions involving hydrogen motion do exhibit a fair degree of quantum effects, reactions involving heavier atoms may be accurately described using approximate methods. Considering that the size of chemical systems of interest today can contain thousands of atoms (such as DNA), methods other than quantum mechanics must be used for calculating the physical properties of those systems.

Many such approximate methods have been developed over time. These include classical as well as semiclassical methods. Two examples of classical methods include classical molecular dynamics and transition state theory. These two theories can be used in fairly large systems. In fact, many scientists use molecular dynamics on systems as large as DNA. Unfortunately, these methods do not include quantum effects. In this work, we look at several examples of semiclassical methods, where the quantum effects are estimated using semiclassical approximations.

In Chapter 2, we present thermal reaction rate calculations obtained using Semiclassical Transition State Theory (SCTST)[15–19]. SCTST is a modification on the original classical transition state theory(TST)[1–3]. Classical TST relies on three fundamental assumptions. First we use the Born-Oppenheimer approximation to assume that the nuclear and electronic motions are separable. Second, the system is treated using classical mechanics. Lastly, no reactive trajectories

recross the dividing surface. Unfortunately, classical mechanics does not allow for tunneling through the barrier. By treating the system semiclassically, we can allow for an approximation to the tunneling rate. Miller and Handy developed just such a method using the good action angle variables at the transition state. In their resulting equations, the reaction rate is a sum of semiclassical tunneling coefficients. In Chapter 2, we note that the semiclassical transmission coefficient can be replaced with the fully quantum mechanical tunneling coefficient for the Eckart barrier. Results are presented for the $H_2 + OH \rightarrow H_2O + H$, $D_2 + OH \rightarrow HDO + D$, and $Cl + H_2 \rightarrow HCl + H$ reactions. We then compare the SCTST results with previous experimental and quantum mechanical rates.

Chapter 3 presents a new look at the dissociation of triple ketene. In the early nineties, Moore and coworkers excited rotationally cold ketene to the S_1 surface[52,53]. The system then underwent an intersystem crossing to the T_1 surface and dissociated. The resulting dissociation rate showed a curious step structure. The steps occurred as the energy of the system was increased. Using RRKM theory, Moore showed that the steps appeared as available channels opened up in the transition state. However, this explanation has not withstood scrutiny. A few years ago Gezelter and Miller performed calculations on the system, but they were unable to reproduce the structure[63]. They listed three hypotheses as to the source of the step structure in the rate. (1) There is more than one transition state along the reaction path. (2) The potential surface that Gezelter used was not sufficiently accurate. (3) The system experiences intersystem crossings at or near the transition state. Allen and coworkers have recently made available a more complete potential surface, evaluated using CCSD(T)[71]. We use this new surface to try to reproduce the step structure. We hope that by utilizing this new surface, we will gain insight into the underlying principles that give rise to the step structure in the dissociation rate.

Finally, in Chapter 4 we apply Semiclassical Initial Value Representation (SCIVR) methods to a model system[79,80]. Specifically, we examine the Herman-

Kluk IVR[81,82], where the propagator is represented as a phase space average. This phase space integral is calculated using Monte Carlo techniques, but unfortunately the integrand can be highly oscillatory. This makes convergence using Monte Carlo difficult (if not impossible) within a reasonable amount of computer time. In addition, for chaotic systems, the magnitude of the integrand can become too large for the computer to handle. This is due to the pre-exponential factor, which is a function of the monodromy or stability matrix. The more chaotic the system, the greater the change in position at time t given a change in the initial position at time 0. Hence, methods for smoothing the integrand would be very useful and might allow calculations on previously intractable problems. In an attempt to derive a more well behaved integrand, we introduce identity in the form of a time integral. We also use the adiabatic approximation to evaluate the monodromy matrix in order to simplify our resulting equation for the spectrum of our system. We apply our method to a model system of two harmonic oscillators interacting via a quartic coupling term. Results are presented for the non-interacting oscillators as well as increasing levels of coupling.

Chapter 2

Semiclassical Transition State Theory

2.1 Introduction

Classical Transition State Theory (TST)[1–9] provides a simple way to calculate the thermal reaction rates of gas phase reactions. In the TST formalism, the rate is equal to the flux across a dividing surface in coordinate space. This dividing surface separates the product and reactant regions. It is placed at the transition state (or saddle point) along the minimum energy path between the reactants and products. Using mass weighted coordinates, the minimum energy path is the steepest decent path, from the saddle point to the reaction and product regions. It is obtained by following the negative of the gradient. The fundamental assumption of classical TST is that trajectories cross the diving surface only once. Thus classical TST would yield the exact classical thermal rate constant if the reaction path had a bottleneck that did not allow for returning trajectories. Unfortunately, many chemical systems do result in trajectories that recross the dividing surface. Some features that might cause such trajectories include having more than one transition state along the reaction path or forming long lived collision complexes. When trajectories do recross the dividing surface, classical TST is an upper bound to the classical thermal rate.

Several other assumptions are included in TST. First is a separation of the electronic and nuclear motion, a typical assumption for theoretical calculations. Secondly, the system is also assumed to obey classical mechanics. This can be an unreasonable assumption when light atoms such as hydrogen are involved in the reaction, especially at low temperatures where quantum effects can be significant. A third assumption is the separability of the orthogonal modes at the transition state. However for certain reactions the couplings between the reaction path and the orthogonal modes can be quite large and may influence the thermal reaction rate. We seek to modify TST to account for some of these deficiencies.

Due to the simplicity of using transition state theories for calculating thermal reaction rates, many versions of TST have been derived. One popular method has been to vary the location of the diving surface in order to provide the lowest upper bound for the thermal rate[10–14]. One such method involves computing the optimal dividing surface for each total energy. This is referred to as microcanonical variational TST. A second approach is canonical variational TST, where the best dividing surface is found for all total energies and angular momenta that contribute to the thermal rate . This is in no way meant to be an exhaustive list of transition state theories in current use. Many review articles have been written about variations of classical TST that the reader might find informative.

Handy and Miller have derived the Semiclassical Transition State Theory (SCTST)[15–19], where the rate is a function of the transmission probabilties through each quantum state at the transition state. These transmission coefficients treat the reaction path with a semiclassical approximation, which gives a better description of the tunneling dynamics and leads to more accurate reaction rates. The semiclassical transmission coefficients are expressed as a function of the locally conserved action variables at the transition state. This allows for coupling between the reaction path and the orthogonal degrees of freedom. The couplings can have a substantial impact on the rate if the curvature of the reaction path is large. We also include anharmonic terms in the potential energy, which provides

a better parameterization of the true potential surface further from the transition state than a purely harmonic analytical potential.

2.1.1 The Rate Equation

The thermal rate for a reaction can be expressed as a boltzmann average of the cumulative reaction probability[20–22] (CRP)

$$k(T) = \frac{1}{(2\pi\hbar Q_r)} \int dE e^{-\beta E} N(E), \tag{2.1}$$

where Q_r is the reactant partition function per unit volume, and β is inversely proportional to the temperature in the common definition $\left(\beta = \frac{1}{kT}\right)$. The reactant partition function is calculated using the traditional rigid-rotor harmonic oscillator approximation.

Using the semiclassical approximation we express the CRP as a sum over the tunneling probabilities through a given quantum state, $\mathbf{n}^\ddagger$,

$$N(E) = \sum_{\mathbf{n}^\ddagger} P(\mathbf{n}^\ddagger, E), \tag{2.2}$$

where the tunneling probabilities are functions of the barrier penetration integral (θ)

$$P(\mathbf{n}^\ddagger, E) = \frac{1}{1 + e^{2\theta(\mathbf{n}^\ddagger, E)}}. \tag{2.3}$$

The previous equations give us a simple expression for calculating thermal reaction rates for states with zero angular momentum. For $J \neq 0$ states the cumulative reaction probability can again be written as a sum of tunneling probabilities

$$N(E) = \sum_{\mathbf{n}^\ddagger, \mathbf{J}, \mathbf{K}} P_{J,K}(\mathbf{n}^\ddagger, E), \tag{2.4}$$

where we sum over all quantum states and rotational levels. The individual tunneling probabilities are calculated by adding the rotational energy to Equation 2.8

$$E = E(\mathbf{n}^\ddagger) + E_{J,K} \tag{2.5}$$

Since the functional form of the rotational energy is dependent on the geometry of the system, we set it aside for now. We will revisit the issue for each chemical reaction that we investigate. All that remains is deriving an expression for θ. We adopt atomic units from here on out, such that $\hbar = 1$.

In this chapter we apply SCTST to two chemical reactions in order to calculate the thermal reaction rates. In Section 2.2 we introduce SCTST and derive the necessary equations. We modify SCTST to include the quantum mechanical tunneling coefficient in Section 2.3. We present background and results on the $OH + H_2 \rightarrow H_2O + H$ and $Cl + H_2 \rightarrow ClH + H$ reactions in Section 2.4. We find that SCTST gives excellent agreement with experimental and fully quantum mechanical results. Section 2.5 concludes.

2.2 Semiclassical Transition State Theory

At a minimum on a potential energy surface, we perform an expansion in terms of the normal coordinates (Q_k) up to fourth order

$$V = V_0 + \frac{1}{2}\sum_{k}^{F} \omega_k^2 Q_k^2 + \frac{1}{6}\sum_{k,l,m}^{F} f_{klm} Q_k Q_l Q_m + \frac{1}{24}\sum_{k,l,m,n}^{F} f_{klmn} Q_k Q_l Q_m Q_n + \ldots, \tag{2.6}$$

where V_0 is the potential energy at the minimum, and F is the dimensionality of the problem ($F = 3N - 6$, where N is the number of atoms in the system). ω_k are the vibrational frequencies calculated from the force constant matrix, and f_{klm} and f_{klmn} are the third and fourth derivatives of the potential surface at the minimum. The derivatives of the potential energy surface can be calculated from an analytical potential energy surface either numerically or analytically, or from ab initio calculations.

We then use second order perturbation theory[23,24] to derive an expression for

the energy levels in terms of these parameters.

$$E(\mathbf{n}) = V_0 + E_0 + \sum_{k=1}^{F} \omega_k \left(n_k + \frac{1}{2}\right) + \sum_{k \leq l=1}^{F} x_{kl} \left(n_k + \frac{1}{2}\right)\left(n_l + \frac{1}{2}\right), \tag{2.7}$$

where $\left(n_k + \frac{1}{2}\right)$ are the quantum numbers, or in classical mechanics the good action variables for the vibrations[27,28]. E_0 is a spectroscopic constant dependent on f_{klm} and f_{klmn}. x_{kl} are the anharmonic force constants and are also determined from the third and fourth derivatives of the surface at the minimum. Equations used for evaluating the necessary spectroscopic constants have been derived and Handy consolidates them[24–26]. Even though our energy levels are only quadratic in the quantum numbers, this is usually sufficient to obtain accurate results for the vibrational energy levels even at fairly high levels of excitation[29].

Miller has shown that there are also good action variables at a saddle point on the surface[30]. Thus the vibrational energy levels at the transition state can be written in the same format as above.

$$E(\mathbf{n}^{\ddagger}) = V_0 + E_0 + \sum_{k=1}^{F} \omega_k \left(n_k^{\ddagger} + \frac{1}{2}\right) + \sum_{k \leq l=1}^{F} x_{kl} \left(n_k^{\ddagger} + \frac{1}{2}\right)\left(n_l^{\ddagger} + \frac{1}{2}\right), \tag{2.8}$$

where we define mode F as the reaction coordinate, and $\mathbf{n}^{\ddagger}$ denotes the quantum state at the transition state. One should note that the harmonic frequency of the reaction path at the saddle point is completely imaginary. Similarly the anharmonic terms coupling the reaction path to the other orthogonal degrees of freedom, x_{kF}, are also imaginary.

We draw parallels between the quantum number for the reaction path and the barrier penetration integral, θ. For a one-dimensional potential well one uses the Bohr-Sommerfeld quantization rule, which is a semiclassical expression for the quantum number[31]

$$\left(n_F^{\ddagger} + \frac{1}{2}\right)\pi = \int dQ \sqrt{2(E - V(Q))}, \tag{2.9}$$

where again coordinate F is the reaction coordinate. We also know that the barrier penetration integral in an integral of the action through the barrier

$$\theta(E) = \int dQ\sqrt{2(V(Q) - E)}. \tag{2.10}$$

Thus a correspondence between $n_F^\ddagger$ and θ can be seen

$$n_F^\ddagger + \frac{1}{2} \rightarrow \frac{i\theta(E)}{\pi}. \tag{2.11}$$

Using equation 2.8, we replace the quantum number for the reaction coordinate with the above relationship.

$$\begin{aligned} E(\mathbf{n}^\ddagger, \theta) = V_0 + E_0 + \sum_{k=1}^{F-1} \omega_k \left(n_k^\ddagger + \frac{1}{2}\right) + \sum_{k\leq l=1}^{F-1} x_{kl} \left(n_k^\ddagger + \frac{1}{2}\right)\left(n_l^\ddagger + \frac{1}{2}\right) \\ + \left[\sum_{k=1}^{F-1} \bar{x}_{kF} \left(n_k^\ddagger + \frac{1}{2}\right) - \bar{\omega}_F\right] \frac{\theta}{\pi} - x_{FF}\frac{\theta^2}{\pi^2}, \end{aligned} \tag{2.12}$$

where

$$\bar{\omega}_F = \frac{1}{i}\omega_F, \tag{2.13}$$

and

$$\bar{x}_{kF} = \frac{1}{i}x_{kF}. \tag{2.14}$$

This equation for the energy in terms of the barrier penetration integral is inverted to solve for θ at a given energy and a given quantum state. Each θ is then used in conjunction with equations 2.1 through 2.3 to calculate the thermal rates.

The former equations work well if we use only second order perturbation theory, where the energy levels are quadratic in θ. However, if we use a higher level of perturbation theory for the energy levels we obtain an expression for the energy that is of higher order in θ, and the inversion becomes nontrivial. This is also true if the system includes other phenomena such as Fermi resonances. It

would be advantageous to avoid the inversion, and thus make the evaluation of the reaction rate feasible.

We begin by combining equation 2.1 through equation 2.3 and interchanging the order of integration and summation

$$k(T) = \frac{1}{Q_r} \sum_{\mathbf{n}^\ddagger} \int dE e^{-\beta E(\mathbf{n}^\ddagger,\theta)} \frac{1}{1 + e^{2\theta(\mathbf{n}^\ddagger,E)}}. \tag{2.15}$$

Next a change in the integration variable from energy to θ yields

$$= \frac{1}{Q_r} \sum_{\mathbf{n}^\ddagger} \int_{-\infty}^{\infty} d\theta \frac{\partial E}{\partial \theta} e^{-\beta E(\mathbf{n}^\ddagger,\theta)} \frac{1}{1 + e^{2\theta(\mathbf{n}^\ddagger,E)}}. \tag{2.16}$$

This assumes that there is a one-to-one correlation between the energy and θ. Note that the resulting equation is of the same format if this is not the case[32]. Integrating the previous equation by parts and again interchanging the integration and summation yields our final expression

$$= \frac{1}{\beta Q_r} \sum_{\mathbf{n}^\ddagger} \int_{-\infty}^{\infty} d\theta e^{-\beta E(\mathbf{n}^\ddagger,\theta)} \frac{1}{2} sech^2(\theta). \tag{2.17}$$

Similarities between this expression and traditional transition state theory can be seen. TST states that

$$k(T) = kT \frac{Q'_(T)}{Q_r(T)}, \tag{2.18}$$

where Q_r is the reactant partition function, and Q' is the reactive partition function. One can see in our theory that the reactive partition function is a weighted average

$$Q'(T) = \int_{-\infty}^{\infty} d\theta \frac{1}{2} sech^2(\theta) Q(T,\theta), \tag{2.19}$$

where $Q(T,\theta)$ is the pre-reactive partition function

$$Q(T,\theta) = \sum_{\mathbf{n}^\ddagger} e^{-\beta E(\mathbf{n}^\ddagger,\theta)}. \tag{2.20}$$

2.3 SCTST/QM

If we expand equation 2.17 and gather terms, we can make some observation as to the nature of SCTST expression

$$k(T) = \frac{kT}{Q_r}\sum_{\mathbf{n}^\ddagger} e^{-\beta V_{\mathbf{n}}^\ddagger}\int_{-\infty}^{\infty} d\theta \frac{1}{2} sech^2(\theta) e^{-\beta\omega_{\mathbf{n}^\ddagger}\frac{\theta}{\pi}} e^{-\beta(-x_{FF})\frac{\theta^2}{\pi^2}}, \tag{2.21}$$

where

$$\omega_{\mathbf{n}^\ddagger} = \bar{\omega}_F - \sum_{k=1}^{F-1} \bar{x}_{kF}(n_k + \frac{1}{2}), \tag{2.22}$$

and

$$V_{\mathbf{n}^\ddagger} = V_0 + E_0 + \sum_{k=1}^{F-1} \omega_k \left(n_k + \frac{1}{2}\right). \tag{2.23}$$

We see that the expression for the rate includes the semiclassical transmission coefficient for state $\mathbf{n}^\ddagger$ of the activated complex

$$\Gamma_{\mathbf{n}^\ddagger}^{sc} = \int_{-\infty}^{\infty} d\theta \frac{1}{2} sech^2(\theta) e^{-\beta\omega_{\mathbf{n}^\ddagger}\frac{\theta}{\pi}} e^{-\beta(-x_{FF})\frac{\theta^2}{\pi^2}}. \tag{2.24}$$

The reader will recall that the energy at the transition state is quadratic in term of θ using second order perturbation theory. In the case of the Eckart potential, the energy is quadratic in θ for infinite order perturbation theory. Thus it is consistent to replace the semiclassical transmission coefficient in the above equation with the exact quantum mechanical transmission coefficient for the Eckart barrier. One must take care to define the coefficients of θ and θ^2 appropriately, and this gives

$$\Gamma_{\mathbf{n}^\ddagger}^{qm} = e^{\beta V_0}\int_0^{\infty} dE e^{-\beta E} \frac{1}{1 + \frac{cosh^2(\sqrt{\alpha^2 - \frac{\pi^2}{4}})}{sinh^2(\sqrt{\frac{2\pi V_0}{\omega_F}}\sqrt{\frac{2\pi}{\omega_F}})}}, \tag{2.25}$$

where α and μ are the two parameters used by Johnston[33]

$$\mu = \beta\omega_{\mathbf{n}^\ddagger} \tag{2.26}$$

$$\alpha = \frac{\pi}{2} \frac{\omega_{\mathbf{n}\ddagger}}{(-x_{FF})}. \tag{2.27}$$

We change the integration variable from energy to x,

$$k(T) = \frac{kT}{Q_r} \sum_{\mathbf{n}\ddagger} e^{-\beta V_{\mathbf{n}\ddagger}} \frac{\alpha\mu}{2\pi} \int_0^\infty dx e^{-x} \frac{1}{1 + \frac{cosh^2(\sqrt{\alpha^2 - \frac{\pi^2}{4}})}{sinh^2(\sqrt{\frac{2\pi\alpha x}{\mu}})}}, \tag{2.28}$$

where $x = \beta E$.

The evaluation of the rate using the quantum expression for the tunneling requires a quadrature as does the treating the tunneling semiclassically. It is hoped that treating the tunneling quantum mechanically will provide a more accurate tunneling rate through the barrier. However, if the reaction path varies greatly from the shape of Eckart barrier, we may experience a divergence from the experimental rates.

2.4 $H_2 + OH \rightarrow H_2O + H$

2.4.1 Computational Specifics

We use the potential energy surface of Isaacson for the $H_2 + OH \rightarrow H_2O + H$ and $D_2 + OH \rightarrow HDO + H$ reactions[35]. The paper cited gives several parameterizations of a single functional form of the potential function. We use the variant that he labels "Surface 3". The surface reproduces the experimental data of Walch and Dunning[36]. In fact the parameters of this particular formulation of the potential surface have been designed to accurately describe the barrier region. This has positive implications on the accuracy of the anharmonicity of the barrier and the coupling between the modes.

The spectroscopic constants are calculated by Handy and coworkers[18]. They use finite difference differentiation with quadruple precision in order evaluate the constants. The optimal step length is found by finding an island of stability in

the fourth derivatives. The derivatives are entered into SPECTRO[37], a computer program which calculates the necessary constants. Handy and coworkers calculate the force constants in both Cartesian and internal coordinates. They find little difference between calculations using each choice of coordinate systems. Details of the calculations and an in depth discussion of the resulting constants can be found in their paper[18]. Unfortunately, a few minor mistakes are found in the rate calculations in that paper. Current calculations correct for these oversights.

The partition functions are calculated using a harmonic oscillator rigid rotor approximation. The relevant constants are taken from Herzberg[38]. It is found, similar to Handy's calculations, that the partition functions converged by J=9 for the $H_2 + OH$ reaction and J=61 for the $D_2 + OH$ reaction.

The rotational energy levels of our system are solved perturbatively. We use the Watson reduction for the energy levels of an asymmetric top[23]. The elements of the rotational energy matrix are of the form

$$\begin{aligned}\langle J,K|H_J|J,K\rangle = \frac{1}{2}\left(B_v^x + B_v^y\right) J\left(J+1\right) + \left[B_v^z - \frac{1}{2}\left(B_v^x + B_v^y\right)\right] K^2 \\ -\Delta_J J^2 \left(J+1\right)^2 - \Delta_{JK} J\left(J+1\right) K^2 - \Delta_K K^4 \\ +\phi_{JK} J^2 \left(J+1\right) K^4 + \Phi_E K^6, \end{aligned} \tag{2.29}$$

and

$$\begin{aligned}\langle J,K\pm 2|H_J|J,K\rangle = \left[\frac{1}{4}B - D + P\right] \\ \times \left[K_{01}\times K_{12}\right]^{\frac{1}{2}}, \end{aligned} \tag{2.30}$$

where

$$B = B_v^x - B_v^y, \tag{2.31}$$

$$D = \delta_K \left[\left(K\pm 2\right)^2 + K^2\right], \tag{2.32}$$

$$P = \phi_J J^2 (J+1)^2 + \frac{1}{2}\phi_{JK} J (J+1) \left[(K \pm 2)^2 + K^2\right] + \frac{1}{2}\phi_K \left[(-K \pm 4)^2 + K^4\right], \tag{2.33}$$

$$K_{01} = J (J+1) - K (K \pm 1), \tag{2.34}$$

$$K_{12} = J (J+1) - (K \pm 1)(K \pm 2). \tag{2.35}$$

This matrix is diagonalized for each value of J and the energy levels are inserted in the appropriate equations above. The constants used in calculating the rotational energy levels are also calculated using the SPECTRO program and can be found in Handy's paper[18].

2.4.2 Results

Results for the $H_2 + OH$ and $D_2 + OH$ reactions are shown in Figures 2.1-2.4. The theoretical results are compared to the experimental results of Ravishankara[39]. No experimental results are available for the J=0 case, but we have included a plot of J=0 data to emphasize the contribution of nonzero angular momentum states to the thermal rates.

Figure 2.1 shows the zero angular momentum contribution to the rate for the $H_2 + OH$ reaction. The J=0 partition functions are used to calculate these rates. The results designated with the boxes show the effect of using a harmonic potential. One can see that using a harmonic potential significantly raises the rate. This means that the true barrier is wider than the harmonic equivalent. Even with only the J=0 contributions the rate is already too large at all temperatures, but especially at low temperatures. This shows the importance of using an anharmonic potential surface. On the other hand, the SCTST results appear promising. SCTST using the semiclassical (quantum) tunneling coefficient are denoted by circles (stars) and a dashed (dotted) line. We maintain this convention for all graphs.

Figure 2.2 shows the converged thermal reaction rates using all the above methods. We see that the SCTCT does indeed do an excellent job at calculating the rates. This reaction is one of the most challenging to the SCTST method due to the large quantum effects associated with hydrogen motion. At higher temperatures where the contribution from tunneling effects are less important the theoretical values fall within experimental uncertainty. Notice that at very low temperatures, the SCTST methods have underestimated the thermal rates. However, the use of the quantum tunneling coefficient has significantly increased the accuracy over the semiclassical tunneling coefficient at 298 K.

We see similar trends with the $D_2 + OH$. For J=0, the harmonic potential presents us with a barrier that is also too narrow. Figure 2.4 shows that the calculated thermal reaction rates using the anharmonic potential fall well within experimental uncertainty. Even at low temperatures, SCTST yields accurate results. We see that using the quantum tunneling coefficient again increases the reaction rate, but to a much lesser degree than the previous reaction. This is reasonable since less tunneling occurs in the deuterated species.

2.5 $Cl + H_2 \rightarrow HCl + H$

2.5.1 Computational Specifics

The $Cl + H_2 \rightarrow HCl + H$ reaction plays a important role in atmospheric chemistry[40,41]. It has been studied extensively both experimentally[40] and theoretically[41–44]. In our calculations, we use a potential energy surface from Truhlar and coworkers[43]. The reaction occurs through a linear transition state. This surface has been used in several theoretical investigations[42–44].

We calculate the derivatives of the potential energy surface in Cartesian coordinates. Again we use finite difference differentiation with quadruple precision, and the optimal step length is found by finding an island of stability in the fourth

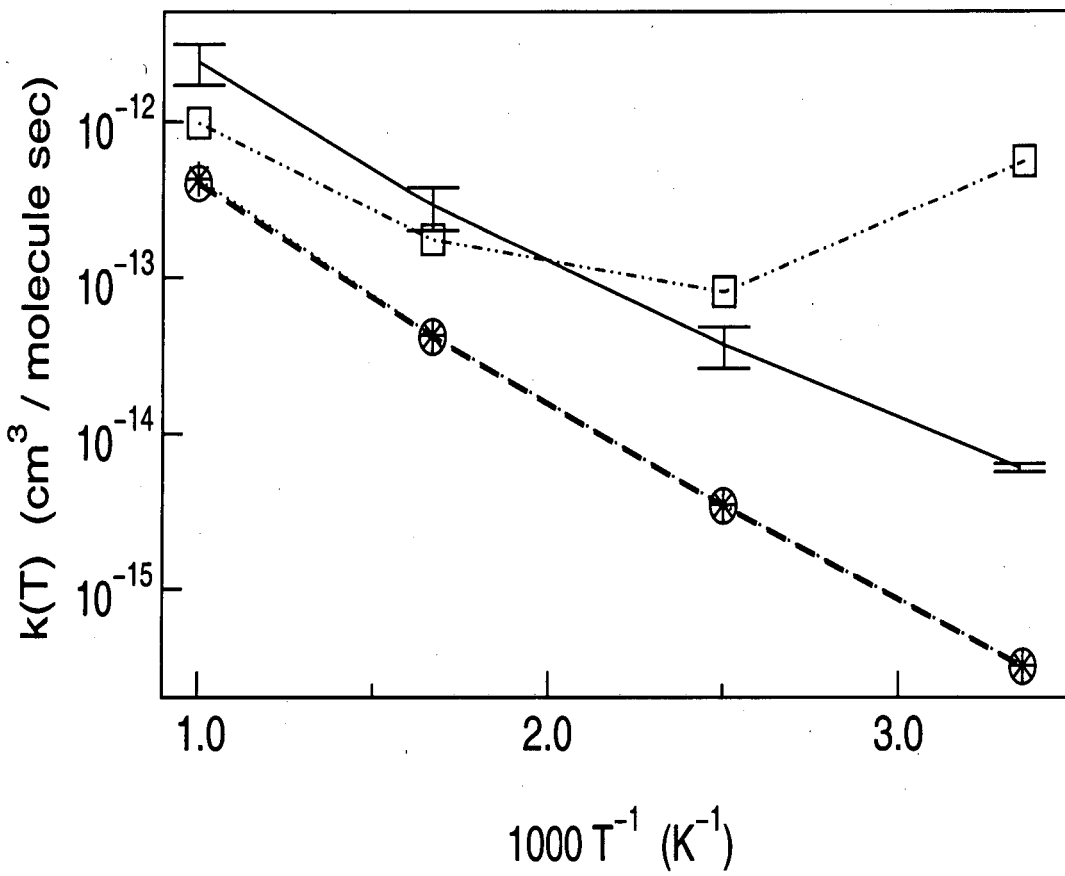

Figure 2.1: Thermal rates for the $H_2 + OH \rightarrow H_2O + H$ reaction with zero angular momentum. Results are shown for temperatures of 298, 400, 600, and 1000 K. SCTST results are shown as circles connected by a dashed line, SCTST with a harmonic potential as boxes connected by a dashed-dotted line, and SCTST with the quantum tunneling coefficient as stars connected by a dotted line. The solid line is the experimental results of Ravishankara[39].

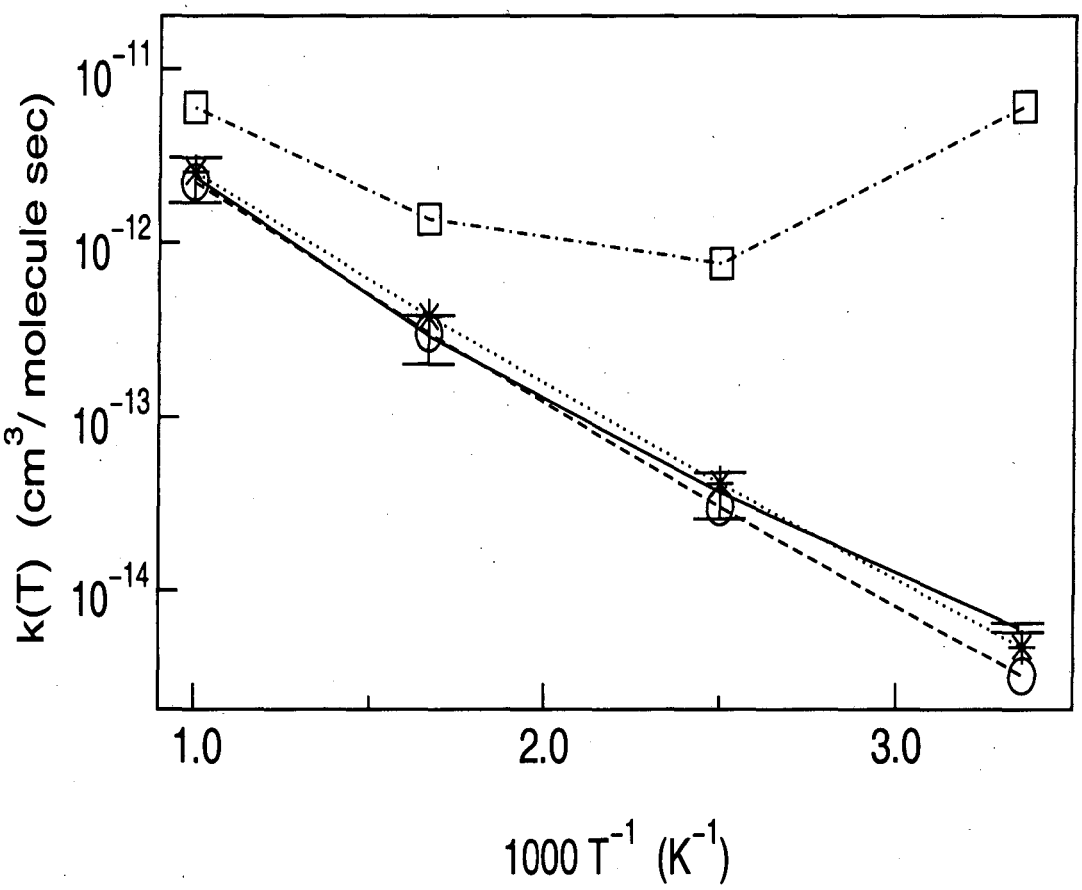

Figure 2.2: Thermal rates for the $H_2 + OH \rightarrow H_2O + H$ reaction. Results are shown for temperatures of 298, 400, 600, and 1000 K. SCTST results are shown as circles connected by a dashed line and SCTST with the quantum tunneling coefficient as stars connected by a dotted line. The solid line is the experimental results of Ravishankara[39].

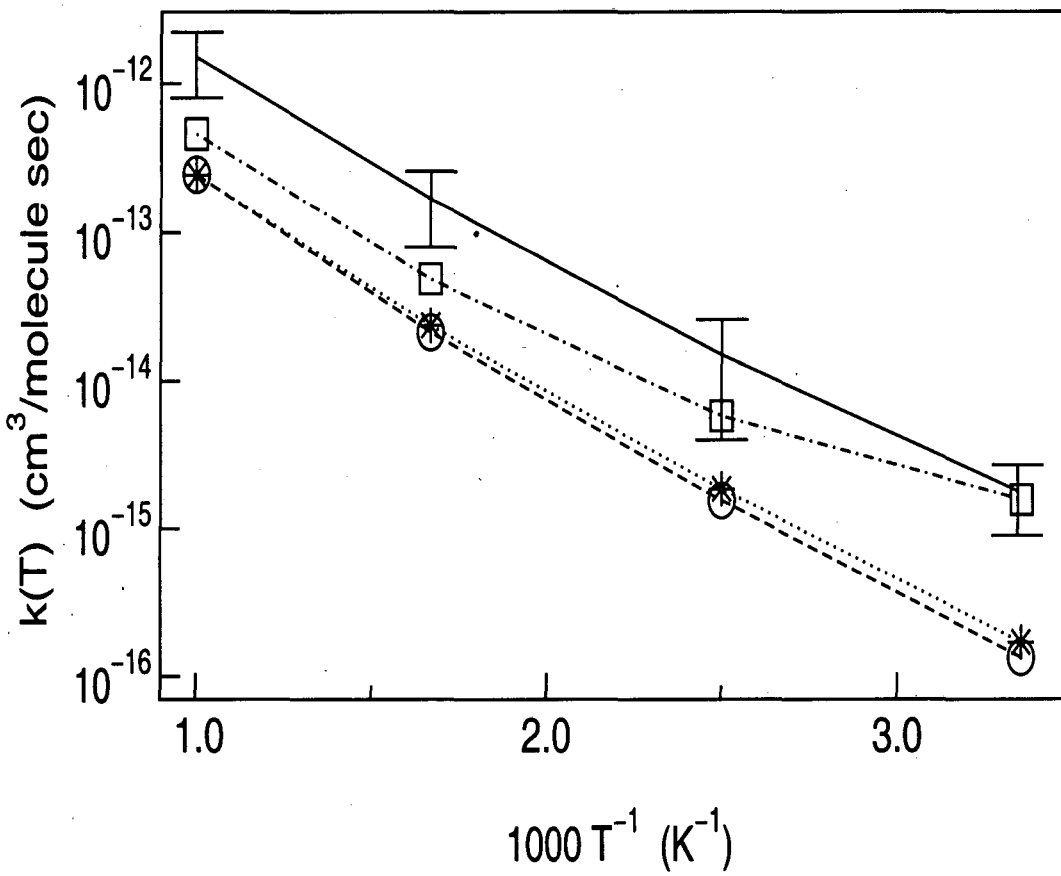

Figure 2.3: Thermal rates for the $D_2 + OH \rightarrow HDO + H$ reaction with zero angular momentum. Results are shown for temperatures of 298, 400, 600, and 1000 K. SCTST results are shown as circles connected by a dashed line, SCTST with a harmonic potential as boxes connected by a dashed-dotted line, and SCTST with the quantum tunneling coefficient as stars connected by a dotted line. The solid line is the experimental results of Ravishankara[39].

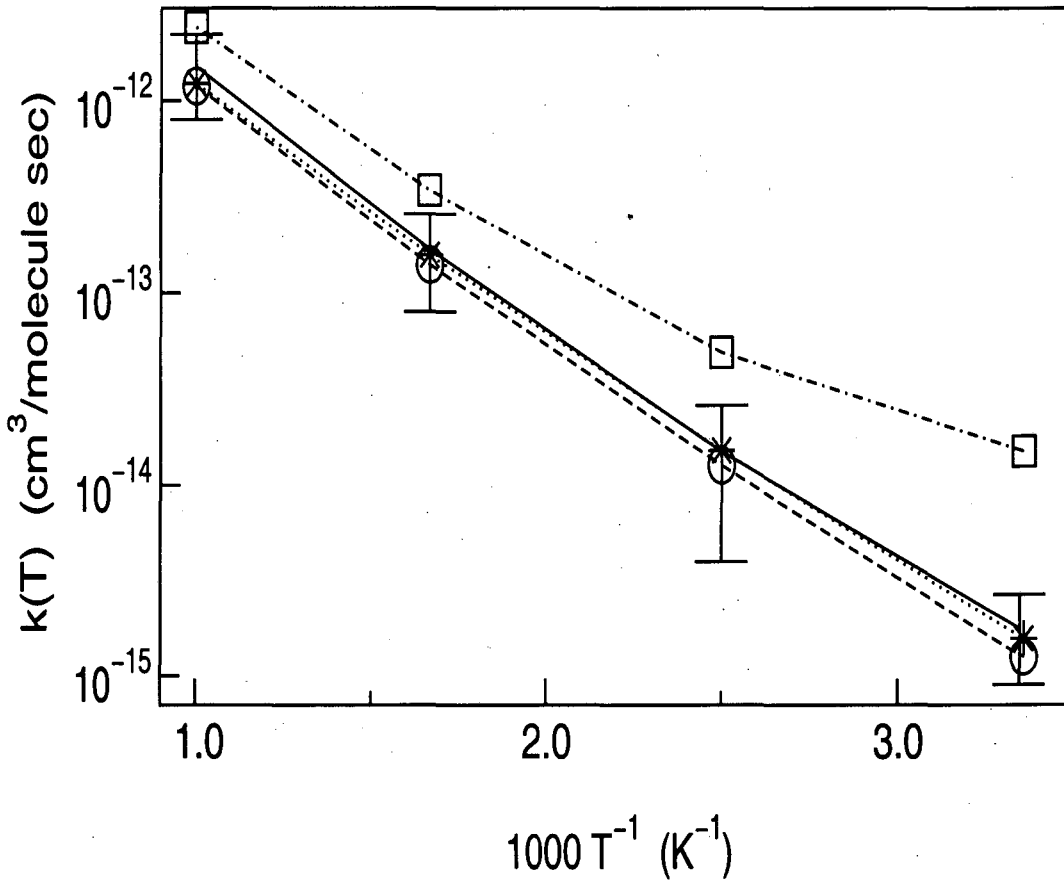

Figure 2.4: Thermal rates for the $D_2 + OH \rightarrow HDO + H$ reaction. Results are shown for temperatures of 298, 400, 600, and 1000 K. SCTST restult are shown as circles connected by a dashed line and SCTST with the quantum tunneling coefficient as stars connected by a dotted line. The solid line is the experimental results of Ravishankara[39].

derivatives. The derivatives are then entered into SPECTRO[37], which calculates the necessary spectroscopic constants. The partition functions are calculated using the harmonic oscillator rigid rotor approximation, and the relevant constants are taken from Herzberg[38].

The rotational energy levels of a linear system are expressed as a truncated sum

$$E(J,L) = B_v \left[J(J+1) - L^2\right] - D_J \left[J(J+1) - L^2\right]^2 + H_J \left[J(J+1) - L^2\right]^3, \tag{2.36}$$

where L is the vibrational angular momentum quantum number for the degenerate mode. Note that there is a twofold degeneracy associated with L, and a (2J+1) degeneracy associated with M. Therefore, the reaction probabilities are multiplied by (2J+1) for L=0 states and 2(2J+1) for L≠0 states.

2.5.2 Results

Figure 2.5 compares SCTST results for the thermal reaction rates to the true quantum results of Wang and coworkers[42]. Wang performed a full dimensional quantum calculation using this same potential surface. His results are denoted by the solid line. We maintain the same convention in labeling our plots ; SCTST results using the semiclassical (quantum) tunneling coefficient are denoted by circles (stars) and a dashed (dotted) line. From our previous results we have seen that an anharmonic potential surface is necessary, and we have found a similar effect with this reaction. Again the semiclassical tunneling coefficient leads to an underestimation of the rate. However, the quantum tunneling coefficient greatly improves the accuracy of SCTST especially at lower temperatures where the role of tunneling is greater. In fact the quantum SCTST rates are quite good for this reaction.

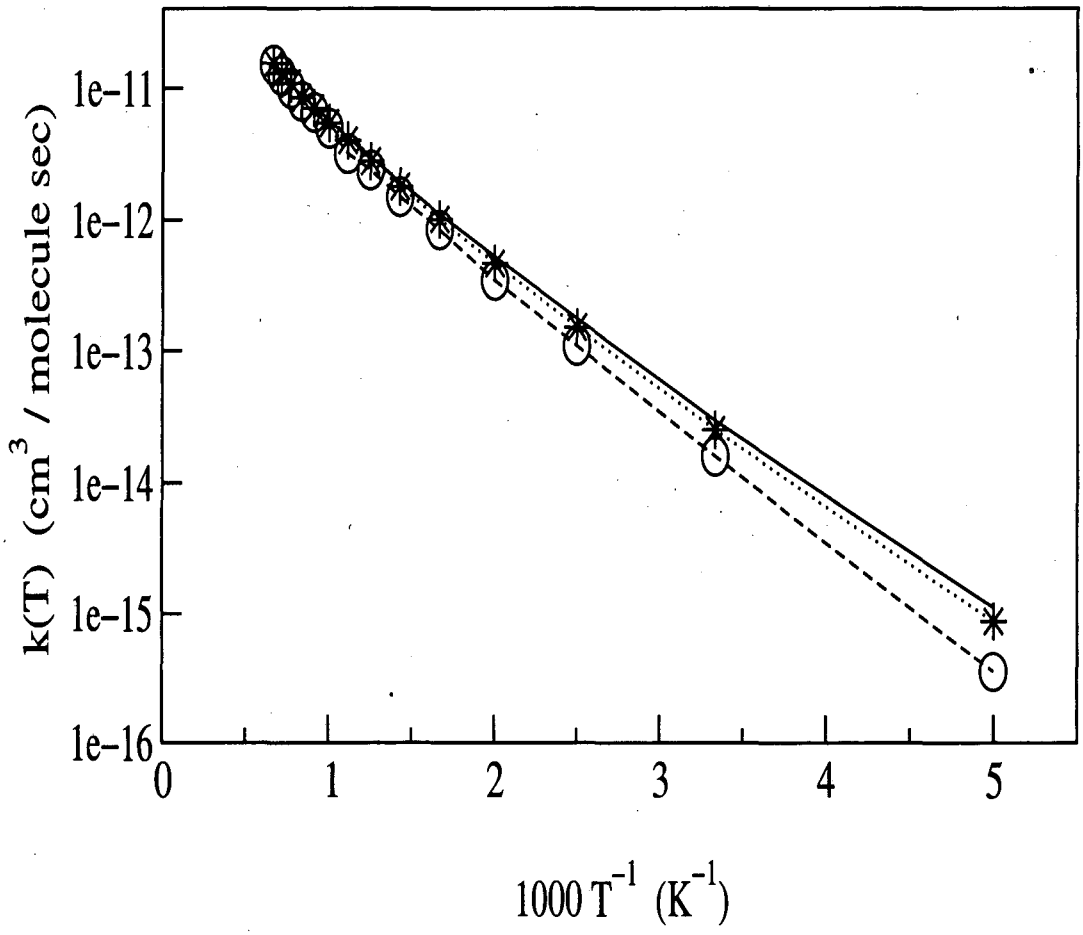

Figure 2.5: Thermal rates for the $Cl + H_2 \rightarrow HCl + H$ reaction. Results are shown at temperatures for intervals of 100 K, beginning at 200 K. SCTST results are shown as circles connected by a dashed line, and SCTST with the quantum tunneling coefficient as stars connected by a dotted line. The solid line is the fully quantum results of Wang and Miller[42].

2.6 Conclusions

We have seen that Semiclassical Transition State Theory provides an inexpensive and fairly accurate way of calculating thermal reaction rates. SCTST improves on classical TST by allowing tunneling through the barrier using a semiclassical or quantum description. The method allows the use of an anharmonic potential, and includes the effects of coupling between the reaction path and the orthogonal degrees of freedom. Results using SCTST generally fall within experimental error and agree well with full quantum results. Unlike full quantum calculations, the scalability of SCTST makes the calculation of rates for large systems feasible. SCTST can be a valuable tool for calculating rate constants for a variety of reactions.

Chapter 3

Dissociation of Triplet Ketene

3.1 Introduction

The dissociation of ketene has been a topic of interest in the past few years. Various aspects of reactive and non-reactive processes involving the molecule have been studied at length both experimentally[45–60] and theoretically[61–67].

By labeling the carbon atoms in ketene, Moore and coworkers saw an intriguing energy dependence in the internal isomerization rate of ketene through the oxirene intermediate[52,53]. Gezelter and Miller performed theoretical calculations to identify the basis for the energy dependence of the isomerization[63]. Although they obtained results qualitatively similar to experiments, they were unable to draw any definite conclusions as to the source of the structure.

The dissociation of ketene is the main aspect of focus in the chemical community. While some studies have examined the dissociation on the singlet surface, where there is no barrier to recombination of the products[56–62], more recently attention has been lavished on the dissociation on the triplet surface[54,55,63]. The dissociation on the triplet surface is a simple barrier process. We examine the dissociation of triplet ketene onto the triplet methylene surface in this chapter.

Moore and coworkers use a super sonic molecular jet to prepare rotationally cold ketene on the S_0 (ground state singlet) surface at around 5 degrees K. They use a UV laser to excite these rotationally cold molecules onto the S_1 (first excited singlet) surface at the dissociation threshold. The ketene then undergoes an intersystem crossing to the T_1 (triplet) surface and dissociates. In order to detect the rate of reaction, Moore et al. use laser-induced fluorescence to detect the CO molecule. The resulting rate shows a definite step structure in the energy dependence that results from the opening of new channels at the transition state.

Initial RRKM calculations seemed to explain the structure seen in the dissociation rate. However, these calculations have not withstood recent scrutiny. In order to resolve the origin of the step structure, Gezelter and Miller performed quantum mechanical calculations of the dissociation rate of triplet ketene. Unfortunately, the potential surface available to them at that time was at a low level of theory, and only the stationary points on the surface had been mapped. As a result they were unable to reproduce the step structure of the rate. In their paper they determined that the barrier frequency was too large to reproduce the step structure. They showed that the reaction barrier frequency would need to be on the order of 100 cm^{-1} in order to reproduce the desired structure. In their paper Gezelter and Miller suggested three hypotheses as to why they did not see the step structure. Hypothesis 1: A second transition state is present further out in the product region. Hypothesis 2: The current ab initio surface is not sufficiently accurate. Hypothesis 3: The singlet and triplet surfaces have an intersystem crossing near the transition state. The last hypothesis was suggested by Troe and Moore[68]. In this chapter we use a newly available, highly accurate potential energy surface to evaluate these hypotheses.

The microcanonical dissociation rate is a function of the cumulative reaction probability (CRP)

$$k_d(E) = \frac{N(E)}{2\pi\rho(E)}, \tag{3.1}$$

We calculate the CRP quantum mechanically and semiclassically in this chapter in an attempt to illuminate the processes behind the step structure seen in the dissociation rate. In the above equation, ρ is the density of reactant states per unit energy. In theoretical calculations, one generally uses a rigid-rotor, harmonic oscillator approximation for the density of states. However, Moore has determined that the actual density of states for ketene is two to four times as big as the rigid- rotor harmonic oscillator treatment predicts[69,55]. As a result, Allen has derived a new expression for the density of states from the number of reactant vibrational states available[70]. The number of states available is fit to a functional form

$$lnN = f(E)\sqrt{E - E_0}, \tag{3.2}$$

where

$$f(E) = a + bE + c\exp -dE \tag{3.3}$$

which is then differentiated analytically. The constants in the previous equations are found in Table 3.1. The resulting equation for the density allows for anharmonicity in the potential surface.

We describe a new potential energy surface for the dissociation of triplet ketene in Section 3.2. Section 3.3 elaborates on the methods used to calculate the CRP. We use a quantum scattering methodology with a Discrete Variable Representation (DVR) and Absorbing Boundary Conditions (ABC) to calculate the CRP quantum mechanically, and the Semiclassical Perturbation (SCP) and Infinite Order Sudden (IOS) approximations for the corresponding semiclassical calculations. The resulting dissociation rates are presented in Section 3.4, and Section 3.5 concludes.

3.2 Potential Energy Surface

We use the triplet ketene fragmentation surface of Allen and coworkers[71]. This new surface goes several steps beyond any surface that has been available in the

Eo	7231.1
a	.1161
b	−2.8581 (−7)
c	−.29487
d	3.1621 (−4)

Table 3.1: Parameters for use in calculating the reactant partition function of ketene. Units are consistent with energies in cm^{-1}.

past. The stationary structures of the reaction are computed using a TZ(2d1f,2p) basis set at a coupled-cluster singles and doubles [CCSD] level. In addition, the potential energy along the reaction path is determined using coupled-cluster methods through triple excitations [UCCSD(T)] with a cc-pVQZ/TZ basis set. Allen and coworkers have calculated not only the stationary structures at these high levels of theory, but they have also provided a parameterization of all constants necessary for the evaluation of the reaction path hamiltonian. The one-dimensional form of the potential energy surface as a function of the reaction path is

$$\begin{aligned} V[R(s)] = &-d_1 + d_1\left[1 - e^{-c_1(R-R_1)}\right]^2 \\ &+d_2 Sech[c_2(R(s) - R_2)] + d_3 Sech[c_3(R(s) - R_3)], \end{aligned} \tag{3.4}$$

where,

$$R(s) = R_0 + P_6(s)[1 + P_5(s)]^{-1}, \tag{3.5}$$

and

$$P_n(s) = \sum_{m=1}^{n} c_m (s - s_0)^m. \tag{3.6}$$

Ro	1.44637
So	−4.12
d1	−1.6785
d2	6.585 (−1)
d3	1.0383
c1	−7.97 (−3)
c2	1.34 (−1)
c3	−3.410 (−1)
c4	3.174 (−1)
c5	−4.597 (−3)
c6	5.739 (−4)

Table 3.2: Parameters for calculating the potential energy along the reaction path. Units are consistent with energies in cm^{-1}.

Parameters for the previous equations are shown in Table 3.2. All other constants for the calculation of the full dimensional potential surface are supplied by a subroutine available from Allen.

The transition state configuration is shown in Figure 3.1, where the C-C critical bond distance is 2.257 $\AA$. Over the course of the reaction the C-O bond contracts from 1.1863 $\AA$ to 1.1252 $\AA$, and the H-C-H angle increases from 120.13 degrees to 133.48 degrees. Notice that at the transition state the system has already undergone 86 % and 78 % of its change in these two coordinates. Allen also

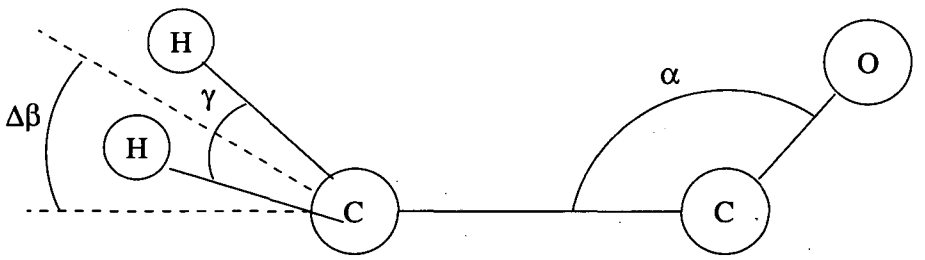

R(C–C)=2.1835

R(C–O)=1.1340

R(C–H1)=1.0722

R(C–H2)=1.0743

α=115.42

γ=130.88

Δβ=.087

Figure 3.1: C_s^{II} Transition State of Triplet Ketene. Lengths are in units of $\mathring{A}$ and bond angles are in degrees.

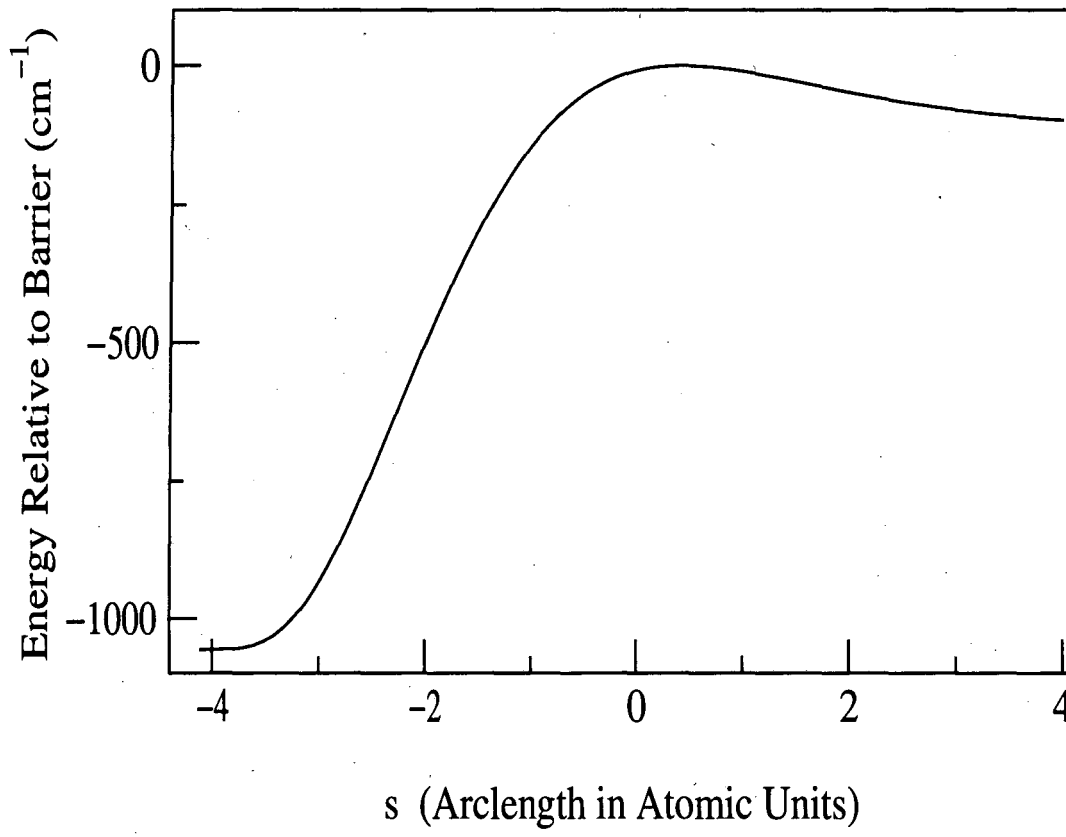

Figure 3.2: One-dimensional potential energy of triplet ketene as a function of the reaction path, s. The arclength is in atomic units. The reaction has a barrier of 1045 cm^{-1}.

sees a monotonic decay in the tail of the reaction path and concludes that there is only one transition state along the reaction path, thus ruling out hypothesis 1 of Gezelter and Miller[63].

Using the singlet-triplet splitting of methylene, Allen finds that the reaction threshold energy is 26969 cm^{-1}. The barrier height of the triplet surface is 1045 cm^{-1}(See Figure 3.2) which lies 115 cm^{-1} above the product region. The reaction path displays a barrier frequency of 321i cm^{-1}, which is much greater than the theoretical value of 100 cm^{-1} that Gezelter found necessary to reproduce the step structure in the rate[63]. However the barrier in the transition state region displays a fair amount of anharmonicity, and Gezelter's calculations assumed a harmonic barrier. The anharmonicity in the reaction path has the effect of widening the barrier, which may or may not result in the appearance of the step structure. Considering the level of theory used in these calculations, Allen has concluded that the barrier frequency is unlikely to be significantly smaller than current calculations and declares hypothesis 3 as improbable.

3.3 Theoretical Methods

3.3.1 DVR-ABC

We use the DVR-ABC methodology for calculating the CRP quantum mechanically. Unfortunately, such grid methods do not scale favorably with an increasing number of dimensions. We therefore perform a one-dimensional calculation and fold in the other degrees of freedom using a canonical transformation

$$N(E) = \sum_{\mathbf{n}=0}^{\infty} N_{1d}\left(E - \epsilon_{\mathbf{n}}^{F-1}\right), \tag{3.7}$$

where

$$\epsilon_{\mathbf{n}}^{F-1} = \sum_{k=2}^{F} \omega_k \left(n_k + \frac{1}{2}\right). \tag{3.8}$$

These calculations are in the same vein as those performed by Gezelter with the previous surface. We present the necessary equations here and point the reader

to Gezelter's paper for a detailed discussion[64,63].

Seideman and Miller[73] showed that the CRP could be written as a quantum mechanical trace

$$N(E) = 4tr\left[\hat{\epsilon}_r^{\frac{1}{2}}\hat{G}(E)\hat{\epsilon}_p\hat{G}(E)\hat{\epsilon}_r^{\frac{1}{2}}\right], \tag{3.9}$$

where $\hat{G}(E)$ is the greens function

$$\hat{G}(E) = \left(E + \hat{H} + i\epsilon\right)^{-1}. \tag{3.10}$$

$\hat{H}$ is the hamiltonian for the system, and ϵ is an absorbing potential that absorbs outgoing amplitude and ensures that the boundary conditions of the wave functions are enforced. ϵ_r is the absorbing potential in the reactant region, and ϵ_p is the corresponding absorbing potential in the product region. The Hamiltonian for our one-dimensional system is

$$\hat{H} = T_s + V(s). \tag{3.11}$$

where V(s) is a diagonal matrix of the potential energy and T_s is the kinetic energy. Using a sinc function DVR basis, the elements of the kinetic energy matrix are

$$\begin{aligned} T_{i,j} &= \frac{(-1)^{i-j}}{2\mu\Delta R^2}\left(\frac{\pi^2}{3} - \frac{1}{2i^2}\right) && i = j, \\ &= \frac{(-1)^{i-j}}{2\mu\Delta R^2}\left(\frac{2}{(i-j)^2} - \frac{2}{(i+j)^2}\right) && i \neq j, \end{aligned} \tag{3.12}$$

where ΔR is dependent on the number of grid points per deBroglie wavelength, N_B

$$\Delta R = \frac{2\pi}{N_B\sqrt{(2\mu(E_{high} - V_{low})}}. \tag{3.13}$$

E_{high} is the highest energy at which we wish to calculate the rate, and V_{low} is the lowest point on the potential energy surface. The absorbing potential is of the form

$$\epsilon_r(R) = a\left(\frac{R_r - R}{R_r - R_{min}}\right)^{z_r} h(R_r - R) \tag{3.14}$$

Rr	2.30
Zr	5
Rmin	1.7
Rmax	3.5
Rp	2.85
Zp	4
a	.02

Table 3.3: Parameters for the calculation of the absorbing potentials. All parameters are in atomic units.

$$\epsilon_p(R) = a\left(\frac{R - R_p}{R_{max} - R_p}\right)^{z_p} h(R - R_p). \tag{3.15}$$

Table 3.1 presents typical values for the parameters of the absorbing potentials.

3.3.2 SCP-IOS

The reader will recall from Chapter 2 that the semiclassical cumulative reaction probability can be expressed as a sum of individual tunneling probabilities (Equation 2.2). Those individual tunneling probabilities are a function of the barrier penetration integral (Equation 2.3). Using the Vibrationally Adiabatic Zero Curvature (VAZC) approximation on the hamiltonian along with energy conservation yields

$$\theta(\mathbf{n}, E) = \int ds\sqrt{2\left(V_{\mathbf{n}}(s) - E\right)}, \tag{3.16}$$

where

$$V_{\mathbf{n}}(s) = V_0(s) + \sum_{k=1}^{F-1} \omega_k(s) \left(n_k + \frac{1}{2}\right). \tag{3.17}$$

Notice that this approximation doesn't allow for an anharmonic reaction path potential, nor does it take coriolis or curvature couplings into account. These curvature couplings can significantly affect the rate. In fact, Truhlar has shown that the VAZC approximation does not yield accurate results for the collinear $H + H_2$ reaction. In the case of ketene, the step structure of the rate is not seen using the VAZC approximation. This might be corrected if we somehow include the coupling between the reaction path and the vibrational modes.

In order to introduce the effects of reaction path curvature, we use the Semi-classical Perturbation and Infinite Order Sudden Approximations in a unified theory derived by Miller[74] (SCP-IOS). We begin by writing the hamiltonian in action-angle variables, $(\mathbf{n}, \mathbf{q})$

$$H(\mathbf{n}, \mathbf{q}, s, p_s) = \frac{\frac{1}{2}\left[p_s - \sum B_{k,k'}(s)\sqrt{(2n_k+1)(2n_{k'}+1)}\sqrt{\frac{\omega_{k'}(s)}{\omega_k(s)}}\sin q_k \cos q_{k'}\right]^2}{\left[1 + \sum_{k=1}^{F-1} B_{k,F}(s)\sqrt{\frac{2n_k+1}{\omega_k(s)}}\sin q_k\right]} + V_0(s) + \sum_{k=1}^{F-1} \omega_k(s)\left(n_k + \frac{1}{2}\right), \tag{3.18}$$

where $\omega_k(s)$ are the harmonic frequencies, $B_{k,k'}(s)$ are the coriolis coupling, and $B_{k,F}(s)$ are the curvature couplings. This is the reaction path formulation of the hamiltonian[75]. The barrier penetration integral according to Miller's paper is expressed in a slightly different form than before.

$$\theta(\mathbf{n}, \mathbf{q_0}) = -p_s(s)s|_{s_1}^{s_2} + \int_{s_1}^{s_2} p_s(s)ds, \tag{3.19}$$

where $s_1 \to -\infty$ and $s_2 \to +\infty$. But a careful inspection proves this is the same as equation 3.16. We then use energy conservation to determine p_s

$$p_s(s) = \sqrt{2(V_{\mathbf{n}} - E)}\left[1 + \sum_{k=1}^{F-1} B_{k,F}(s)\sqrt{\frac{2n_k+1}{\omega_k(s)}}\sin q_k(s)\right] + \sum_{k,k'=1}^{F-1} B_{k,k'}(s)\sqrt{(2n_k+1)(2n_{k'}+1)}\sqrt{\frac{\omega_{k'}(s)}{\omega_k(s)}}\sin q_k \cos q_{k'}, \tag{3.20}$$

where $V_{\mathbf{n}}$ is the adiabatic approximation to the potential

$$V_{\mathbf{n}} = V_0(s) + \sum_{k=1}^{F-1} \omega_k(s) \left(n_k + \frac{1}{2}\right). \tag{3.21}$$

At this point we differ from Miller's original derivation. In his journal article, Miller goes on to express the action-angle variables as functions of s, the reaction path. Instead, we assume that the action-angle variables are independent of s. We also choose to neglect the coriolis coupling, $B_{k,k'}(s)$. Doing so should not affect the rate since the coriolis couplings are often much smaller than the curvature couplings, $B_{k,F}(s)$. Thus the former equation becomes

$$p_s(s) = \sqrt{2(V_{\mathbf{n}} - E)} \left[1 + \sum_{k=1}^{F-1} B_{k,F}(s) \sqrt{\frac{2n_k + 1}{\omega_k(s)}}\right]. \tag{3.22}$$

Substituting this result into our rate equation, the CRP is now

$$N(E) = \sum_{\mathbf{n}} \frac{1}{1 + e^{2\left[\theta(E) - \sum_{k=1}^{F-1} \theta_k(E)\right]}}, \tag{3.23}$$

where

$$\theta_k(E) = \int ds \sqrt{2\left(V_{\mathbf{n}} - E\right)} \sum_{k=1}^{F-1} B_{k,F}(s) \sqrt{\frac{2n_k + 1}{\omega_k(s)}}. \tag{3.24}$$

Notice that we are in effect calculating a correction factor to the barrier penetration integral that accounts for curvature in the reaction path.

3.3.3 J-Shifting

We incorporate angular momentum into our calculations of the CRP by using the J-shifting approximation. This approximation assumes that $P_J(E)$ is merely a shifting of the J=0 probabilities

$$P_J(E) = P_{J=0}\left(E - E_J\right), \tag{3.25}$$

where E_J is the rotational energy of the system. To calculate the rotational energy levels, the J-shifting approximation assumes that the rotational constants

A*	4.297
B*	.244
C*	.224

Table 3.4: The rotational constants of the C_s^{II} transition state for the dissociation of triplet ketene. The constants are in units of cm^{-1}.

along a reaction path are constants. Traditionally the rotational constants at the transition state are used in the calculation. Table 3.4 shows the rotational constants for the dissociation of triplet ketene. These constants are calculated using the transition state in Figure 3.1. Previous calculations have shown that the J-shifting approximation produces rates in excellent agreement with quantum calculations and experiment[78,42].

3.4 Results

Figure 3.3 shows the one-dimensional CRP calculated using DVR-ABC. Both the current results (solid line) and Gezelter's results (dashed line) are shown. Notice that both rise slowly over a long period. The current result rises faster due to a slightly smaller barrier frequency, 321i cm^{-1} versus 371i cm^{-1}. The reaction rates resulting from folding in the other degrees of freedom are denoted as a solid line in Figure 3.4. Notice that the rate still rises smoothly; the step structure is not reproduced. This is expected given the barrier frequency. Gezelter has shown that a decrease in the barrier frequency to 100 cm^{-1} would reproduce the step

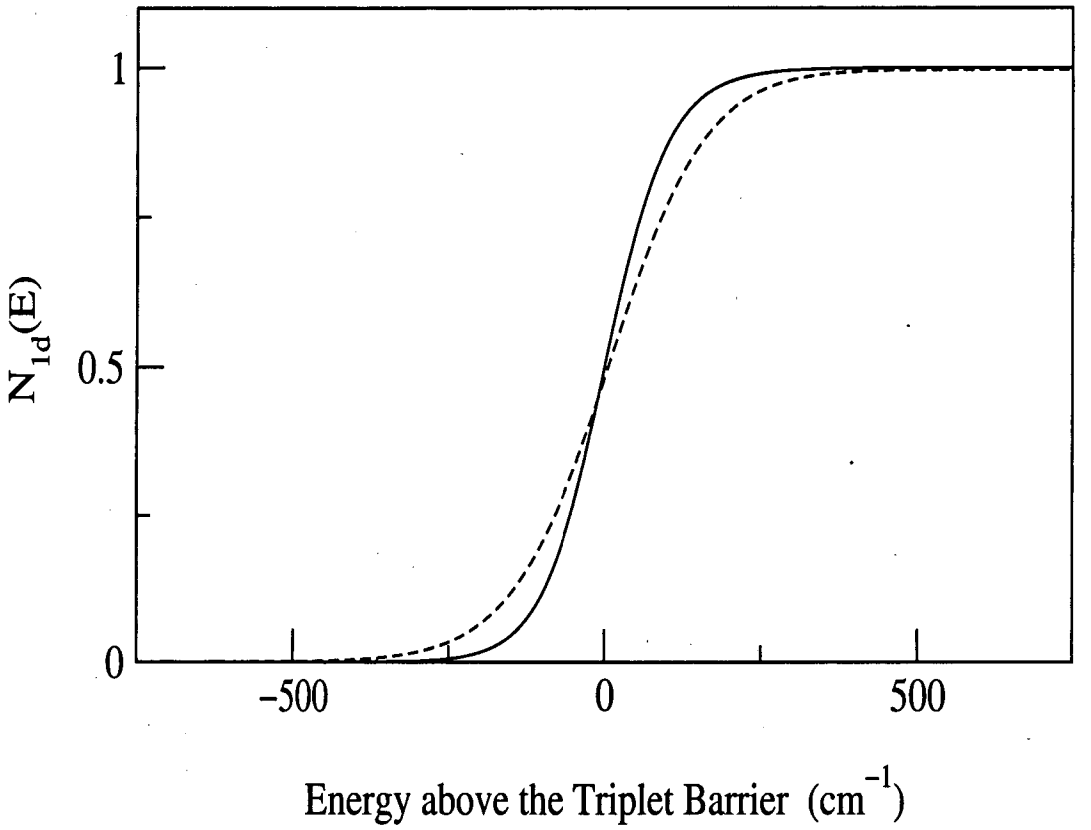

Figure 3.3: The one-dimensional cumulative reaction probability for the dissociation of triplet ketene. The solid line is the result of current calculations. The dashed line is the result of previous calculations by Gezelter and Miller.[63]

structure[63]. This is due to the fact that the frequencies of the vibrational modes are small compared to the barrier frequency. Thus the interval between the steps is smaller than the interval over which the steps rise. While the current potential does predict a wider barrier than the previous surface, the barrier frequency is still not small enough to produce the desired steps.

In Figure 3.4, we have also included the result of SCPIOS but setting all curvature coupling constants to zero (dotted line). Notice that the SCP-IOS with zero curvature agrees qualitatively with the DVR-ABC results. This is logical since the DVR-ABC does not account these couplings. The similarity of the results of these two methods is encouraging. We see that the semiclassical approximation

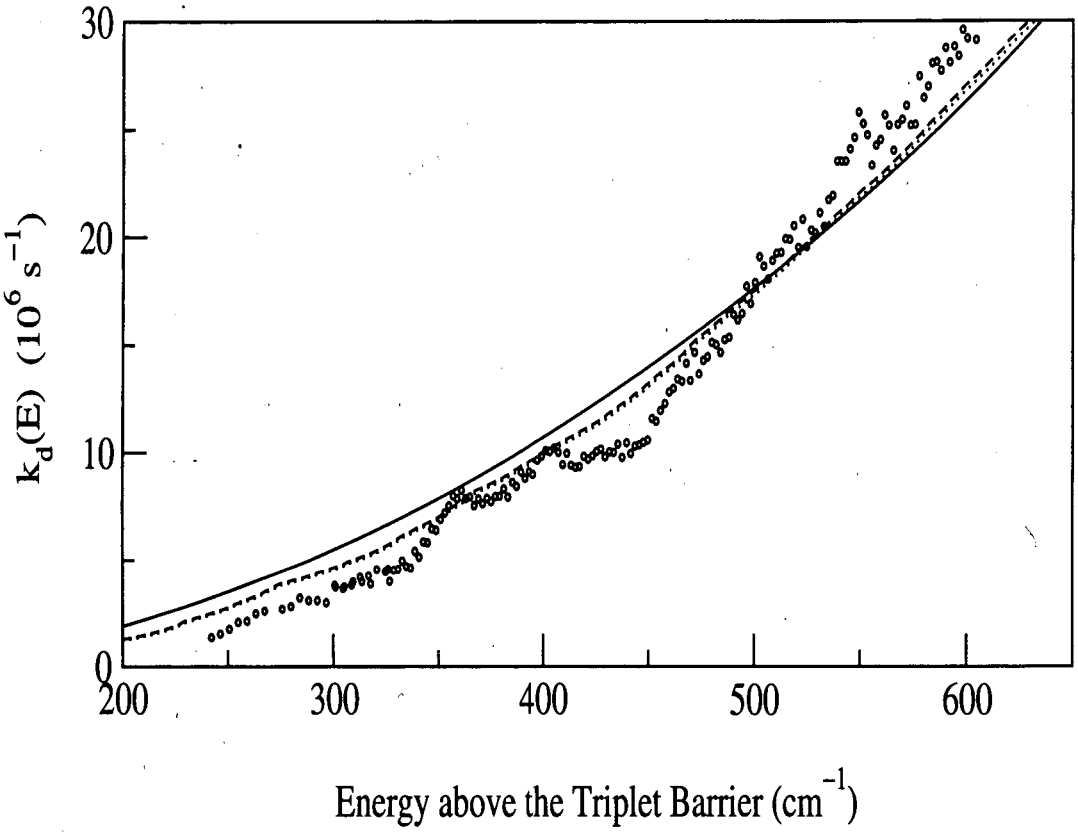

Figure 3.4: The dissociation rate for triplet ketene. DVR-ABC results are shown as a solid line. SCPIOS results are shown as a dashed line. SCPIOS results with no curvature effects are shown as a dotted line. The circles are the experimental results of Moore.[54,55]

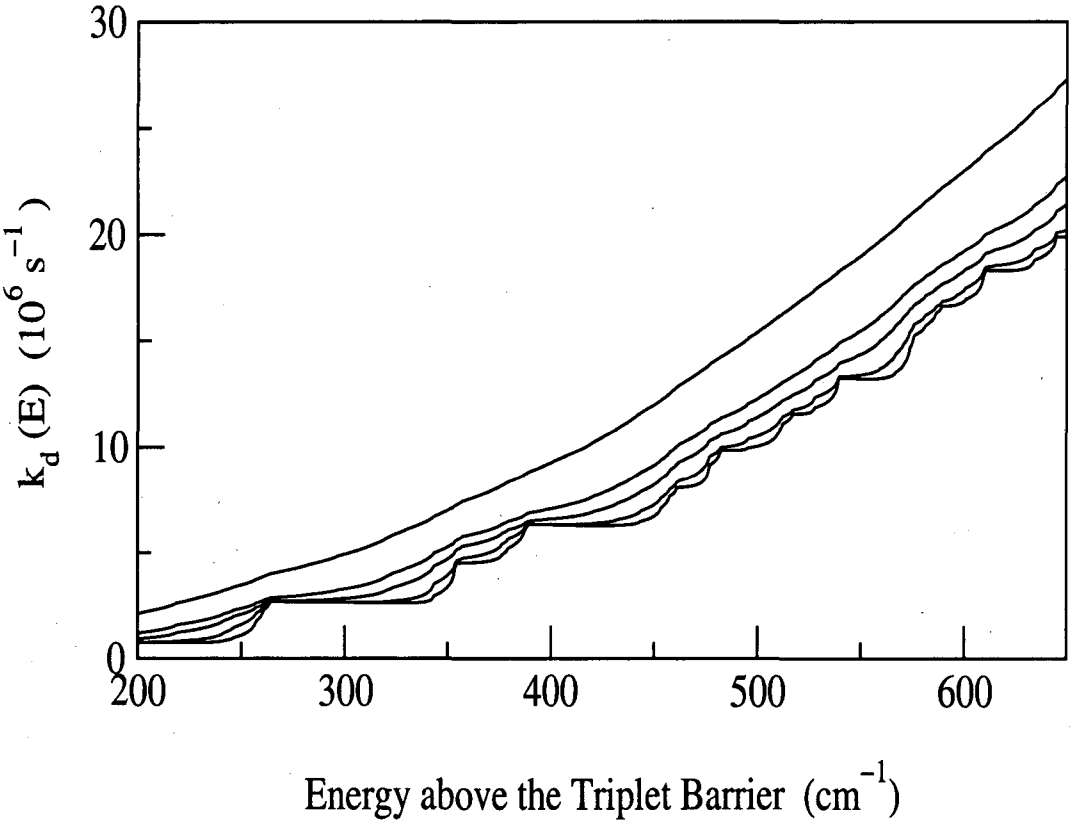

Figure 3.5: The dissociation rates for triplet ketene. The curvature couplings between the reaction path and the orthogonal modes are multiplied a factor of 1, 50, 100, 250, and 500. As the coupling increases the step structure comes into focus.

used in treating the tunneling through the barrier is sufficiently accurate. The dashed line in Figure 3.4 represents the SCP-IOS model described in Section 3.3.2. Notice that both SCP-IOS methods yield similar rates, which means that the curvature of the reaction path has very little effect on the tunneling rate. Again, the reaction rates do not portray the desired step structure.

At what point does the curvature affect the reaction rate? From Equation 3.21 we see that the sum of all θ_k must be on the order of θ in order to affect the barrier penetration integral. Out of curiosity, we multiply all coupling constants by a constant factor. Figure 3.5 shows the reaction rates for these inflated coupling constants. As the curvature of the reaction path increases, we begin to see the step structure appear (See Figure 3.5). Thus we conclude that a reaction path with more curvature would indeed reproduce the step structure seen in experiments.

3.5 Conclusions

In this chapter, we have presented theoretical rates for the dissociation of triplet ketene. These results agree closely with experimental trends. However, the step structure seen in the experiments of Moore[54,55] is not reproduced in our calculations, despite a substantial increase in the accuracy of the potential energy surface.

The current surface is obtained using the latest in *ab initio* methods, and the full reaction path has been mapped. Hence, we are inclined to draw the conclusion that the noticeable absence of the step structure is not due to precision of the potential surface.

In order to reproduce the step structure in the dissociation rate, the effective barrier needs to be wider. In the calculations of Gezelter and Miller, the barrier frequency of the Eckart potential that is necessary to reproduce the desired structure in the rate is 100 cm^{-1}. Current calculations use an analytical form of the

potential surface with a wider barrier. However, this new surface fails to produce the step structure seen in experiments. In order to reproduce the step structure, the effective barrier to reaction must be widened from it's current shape.

As for the question of the existence of a second transition state in the product region, Allen has determined that there is only one transition state. However, a dynamical bottleneck could occur if the perpendicular modes tightened after the transition state. We see no evidence of such an event.

This leaves us with one remaining hypothesis - the crossing of the triplet and the singlet surfaces at a geometry near the transition state. This could give rise to an effective widening of the barrier or some structure in the dissociation rate. Initial studies of the surface crossings have been presented[67]. We await further theoretical studies of the surface interactions. We hope that these studies of the non-adiabatic surfaces will explain the source of the step structure in the dissociation rate of triplet ketene.

Chapter 4

Time Averaging the SCIVR

4.1 Introduction

The Semiclassical Initial Value Representation (SCIVR) has undergone a rebirth of interest recently[79,80]. It presents a practical way to obtain quantum mechanical dynamical properties while restricting the computational complexity, allowing the investigation of more complex chemical systems. The SCIVR approximates quantum mechanical effects while requiring little more than the evaluation of classical trajectories. The Herman Kluk SCIVR[81,82] replaces a quantum mechanical trace with a phase space average over initial coordinates and momenta. The average is then evaluated using Monte Carlo methods. Recent studies have shown the flexibility of the SCIVR, and many encouraging results have been reported[79–113].

However, there are still some difficulties in applying the SCIVR, which have not been completely solved. The main barrier is the evaluation of the phase space integral. The integrand of the SCIVR is highly oscillatory. In chaotic systems, the pre-exponential factor can become quite large. This leads to an integrand that is not only rapidly oscillating but also large in magnitude. As a result of these two factors, Monte Carlo integration methods have trouble efficiently evaluating the integral. Often many millions of trajectories are required for convergence in

highly chaotic systems.

In this chapter we examine the utility of applying time integration to the Herman-Kluk SCIVR. This is an attempt to smooth the integrand, thus improving the rate of convergence. We compare results using the straightforward SCIVR and the time integrated version. Section 4.2 introduces the basic SCIVR in the coherent state formalism. The introduction of the time integration is covered in Section 4.3. Various approximations are applied to simplify the resulting equations and provide an physical understanding of the problem. In Section 4.4 we implement the previous methods using a model system of two harmonic oscillators with a quartic coupling term. The results are presented in Section 4.5, and Section 4.6 summarizes and concludes.

4.2 The SCIVR Formalism

The time correlation function can be used to express many dynamical properties of a molecular system

$$C_{AB}(t) = \mathrm{tr}\left[\hat{A}e^{i\hat{H}t}\hat{B}e^{-i\hat{H}t}\right], \tag{4.1}$$

where the operators and $\hat{A}$ and $\hat{B}$ depend on the molecular quantity of interest. Semiclassically the time evolution operator ,$e^{-i\hat{H}t}$, is replaced by the Herman-Kluk or coherent state SCIVR expression[81,82]

$$e^{-i\hat{H}t} = (2\pi)^{-F}\int d\mathbf{q}_0 \int d\mathbf{p}_0 C_t(\mathbf{q}_0,\mathbf{p}_0)e^{iS_t(\mathbf{q}_0,\mathbf{p}_0)}|\mathbf{p}_t,\mathbf{q}_t,\gamma_t\rangle\langle\mathbf{q}_0,\mathbf{p}_0,\gamma_0|, \tag{4.2}$$

where F is the number of degrees of freedom. $(\mathbf{q}_0,\mathbf{p}_0)$ are the initial positions and momenta of the classical trajectories. $(\mathbf{q}_t,\mathbf{p}_t)$ are the time evolved coordinates and momenta, which are dependent on the initial positions and momenta. γ is an F-dimensional diagonal matrix, where element γ_i is the width parameter for the coherent state of the ith degree of freedom. An individual element of γ can be declared as constant or as a function of time. We will assume for now that γ is a function of time. If γ is instead constant, the equations can easily be simplified.

$C_t(\mathbf{q}_0, \mathbf{p}_0)$ is the pre-exponential factor which is calculated from the elements of the monodromy matrix

$$C_t = \left| \frac{1}{2} \left(\gamma_t^{\frac{1}{2}} \frac{\partial \mathbf{q}_t}{\partial \mathbf{q}_0} \gamma_0^{-\frac{1}{2}} + \gamma_t^{-\frac{1}{2}} \frac{\partial \mathbf{p}_t}{\partial \mathbf{p}_0} \gamma_0^{\frac{1}{2}} - i\gamma_t^{\frac{1}{2}} \frac{\partial \mathbf{q}_t}{\partial \mathbf{p}_0} \gamma_0^{\frac{1}{2}} + i\gamma_t^{-\frac{1}{2}} \frac{\partial \mathbf{p}_t}{\partial \mathbf{q}_0} \gamma_0^{-\frac{1}{2}} \right) \right|^{1/2} . \tag{4.3}$$

$S_t(\mathbf{q}_0, \mathbf{p}_0)$ is the classical action integral along the trajectory

$$S_t = \int_0^t dt \, (p\dot{q} - H) . \tag{4.4}$$

The F-dimensional coherent state wave function in the coordinate space representation is

$$\langle \mathbf{x} | \mathbf{p}_0, \mathbf{q}_0 \rangle = \left(\frac{\gamma_0}{\pi} \right)^{F/4} e^{-\frac{\gamma_0}{2} |\mathbf{x} - \mathbf{q}_0|^2 + i\mathbf{p}_0 \cdot (\mathbf{x} - \mathbf{q}_0)} . \tag{4.5}$$

Unfortunately the integrand in equation 4.2 has proven to be difficult to integrate. It is highly oscillatory and can become quite large due to the pre-exponential factor. Many approaches can be taken to smooth out the integrand. An early solution was to simply throw away the chaotic trajectories if there were only a few such trajectories inhibiting convergence[114]. More recently, Filinov smoothing has proven to be a valuable tool[115–118].

A third method to smooth the integrand involves using the Forward-Backward SCIVR. The trajectory is integrated forward in time to time t, experiences a possible jump in coordinates and/or momenta, and integrated back to time 0[119–123]. If the forward and backward hamiltonians are the same, this method can be applied only when the operator $\hat{B}$ is not unity. Otherwise the trajectory would travel forward and backward along the same path and up at the initial phase point of the trajectory. If the forward and backward hamiltonians are not equal, a phase jump at time t is not imperative, and operator $\hat{B}$ may be unity.

Kay and coworkers have also implemented a time integration scheme for reactive systems, replacing one of the phase space integrals with an integral over

time[124,125]. They have seen a marked improvement in the convergence rates using this method. In the next section we use an integral over time to smooth the integrand. Unlike Kay, we insert identity in the form a time integral, while keeping all phase space integrals. This leads to a severe decrease in the number of trajectories necessary for convergence.

4.3 Time Averaging

The spectrum of a molecule can be written in the standard form as a function of the hamiltonian

$$I(E) = \langle\psi|\delta(E - \hat{H})|\psi\rangle. \tag{4.6}$$

We can express the delta function in its Fourier representation to get an equation of the proper form for implementing the SCIVR

$$I(E) = \frac{1}{\pi} Re \int e^{iEt} \langle\psi|e^{-i\hat{H}t}|\psi\rangle dt. \tag{4.7}$$

Using equation 4.2, our correlation function becomes

$$\begin{aligned}\langle\psi|e^{-i\hat{H}t}|\psi\rangle = (2\pi)^{-F} \int d\mathbf{q}_0 \int d\mathbf{p}_0 C_t(\mathbf{q}_0, \mathbf{p}_0) e^{iS_t(\mathbf{q}_0,\mathbf{p}_0)} \\ \times \langle\psi|\mathbf{p}_t, \mathbf{q}_t, \gamma_t\rangle\langle\mathbf{q}_0, \mathbf{p}_0, \gamma_0|\psi\rangle,\end{aligned} \tag{4.8}$$

Again the integrand is highly oscillatory. We introduce an average over time in order to smooth the integral. This is equivalent to inserting the identity operator as shown below. We simplify the previous equation

$$= \int d\mathbf{q}_0 d\mathbf{p}_0 \frac{1}{T} \left(\int_0^T dt' \right) A(\mathbf{q}_0, \mathbf{p}_0) \tag{4.9}$$

and interchange the order of integration so that the phase space integral is computed first. The result of the phase space integral does not depend on time t'

$$= \frac{1}{T} \int_0^T dt' \langle\psi|e^{-i\hat{H}t}|\psi\rangle. \tag{4.10}$$

The integral over time t' yields T that cancels with the T in the denominator, leaving us with the original result.

Using equations 4.6 and 4.8 and inserting the time integral, the expression for the spectrum becomes

$$I(E) = \frac{1}{T\pi(2\pi)^F} Re \int d\mathbf{q}_0 \int d\mathbf{p}_0 \int_0^T dt \int_t^\infty dt' C_t(t') e^{iS_t(\mathbf{q}_0,\mathbf{p}_0) - S_{t'}(\mathbf{q}_0,\mathbf{p}_0)} \times \langle\psi|\mathbf{q}_{t'}, \mathbf{p}_{t'}, \gamma_{t'}\rangle\langle\mathbf{q}_t, \mathbf{p}_t, \gamma_t|\psi\rangle. \quad (4.11)$$

The pre-exponential factor, actions, and the overlaps correspond to our earlier definitions. However, now we are in essence integrating over trajectories that begin at time t and end at time t'. If we start a trajectory at time 0, then the pre-exponential factor has a new form

$$C_t(t') = \left|\frac{1}{2}\left(\gamma_{t'}^{\frac{1}{2}} \frac{\partial \mathbf{q}_{t'}}{\partial \mathbf{q}_t} \gamma_t^{-\frac{1}{2}} + \gamma_{t'}^{-\frac{1}{2}} \frac{\partial \mathbf{p}_{t'}}{\partial \mathbf{p}_t} \gamma_t^{\frac{1}{2}} - i\gamma_{t'}^{\frac{1}{2}} \frac{\partial \mathbf{q}_{t'}}{\partial \mathbf{p}_t} \gamma_t^{\frac{1}{2}} + i\gamma_{t'}^{-\frac{1}{2}} \frac{\partial \mathbf{p}_{t'}}{\partial \mathbf{q}_t} \gamma_t^{-\frac{1}{2}}\right)\right|^{1/2}, \quad (4.12)$$

where the individual elements in the monodromy matrix are calculated using the chain rule

$$\frac{\partial(\mathbf{q}_{t'}, \mathbf{p}_{t'})}{\partial(\mathbf{q}_t, \mathbf{p}_t)} = \frac{\partial(\mathbf{q}_{t'}, \mathbf{p}_{t'})}{\partial(\mathbf{q}_0, \mathbf{p}_0)} \cdot \frac{\partial(\mathbf{q}_0, \mathbf{p}_0)}{\partial(\mathbf{q}_t, \mathbf{p}_t)}. \quad (4.13)$$

Examining equation 4.11, we see a correspondence between the terms that are factors of time t and those of time t'. Most of the terms dependent on time t are complex conjugates of the terms dependent on time t'. The only term that does not follow this trend is the pre-exponential factor. If the pre-exponential factor was factorable into two parts, and if these two parts were complex conjugates of each other

$$C_t(t') = r(t)e^{i\alpha(t)} r(t') e^{-i\alpha(t')}, \quad (4.14)$$

then the expression for the whole integrand could be factored.

In order to get the pre-exponential factor in the desired format, we evaluate the monodromy matrix using the adiabatic approximation

$$\mathbf{M_{qq}} = \mathbf{L} \cdot \mathbf{\Omega}_t^{-\frac{1}{2}} \cdot \cos\left(\int_0^t \mathbf{\Omega}_t dt\right) \cdot \mathbf{\Omega}_0^{\frac{1}{2}} \cdot \mathbf{L}^T, \quad (4.15)$$

$$\mathbf{M_{qp}} = \frac{1}{m}\mathbf{L}\cdot\mathbf{\Omega}_t^{-\frac{1}{2}}\cdot\sin\left(\int_0^t \mathbf{\Omega}_t dt\right)\cdot\mathbf{\Omega}_0^{-\frac{1}{2}}\cdot\mathbf{L}^T, \tag{4.16}$$

$$\mathbf{M_{pq}} = -m\mathbf{L}\cdot\mathbf{\Omega}_t^{\frac{1}{2}}\cdot\sin\left(\int_0^t \mathbf{\Omega}_t dt\right)\cdot\mathbf{\Omega}_0^{\frac{1}{2}}\cdot\mathbf{L}^T, \tag{4.17}$$

$$\mathbf{M_{pp}} = \mathbf{L}\cdot\mathbf{\Omega}_t^{\frac{1}{2}}\cdot\cos\left(\int_0^t \mathbf{\Omega}_t dt\right)\cdot\mathbf{\Omega}_0^{-\frac{1}{2}}\cdot\mathbf{L}^T, \tag{4.18}$$

where $\mathbf{\Omega}_t$ are the local vibrational frequencies at time t, and $\mathbf{L}$ is the eigenvector matrix. We allow γ to vary with time as a function of the local vibrational frequencies at time t. We choose γ wisely in order to make some cancellations, resulting in a simplified expression for the pre-exponential factor

$$\gamma_0 = m\mathbf{L}\cdot\mathbf{\Omega}_0\cdot\mathbf{L}^T, \tag{4.19}$$

$$\gamma_t = m\mathbf{L}\cdot\mathbf{\Omega}_t\cdot\mathbf{L}^T. \tag{4.20}$$

This choice of γ results in the following pre-exponential factor

$$C_t(t') = e^{-i\int_0^{t'}\sum_k \frac{1}{2}\omega_k(t'')dt''}e^{i\int_0^t\sum_k \frac{1}{2}\omega_k(t'')dt''}. \tag{4.21}$$

From equation 4.21 we see that the pre-exponential factor is in the desired format. We can then factor the pre-exponential factor into two parts that are complex conjugates of each other, leading to an expression for the spectrum that involves only one time integral

$$I(E) = \frac{1}{2\pi T(2\pi)^F}\int d\mathbf{q}_0\int d\mathbf{p}_0\left|\int_0^T e^{iEt}\langle\psi|\mathbf{q}_t,\mathbf{p}_t,\gamma_t\rangle e^{-i\int_0^t[p\dot{q}-\hat{H}-\sum_k\frac{1}{2}\omega_k(t')]dt'}\right|^2 \tag{4.22}$$

According to the previous equation, we have effectively added the zero point energy to the hamiltonian. This is valid for real frequencies, but what happens when imaginary frequencies come into play? We look at a one-dimensional problem for intuitive insight. Take for instance a morse oscillator. When in the

reactive regime, we have a contribution to the zero point energy. However, when the trajectory is at the transition state, there is no contribution to the zero point energy. Is it therefore reasonable to ignore the imaginary frequencies when they occur? In an upcoming section, we present an example of a system that has such frequencies.

4.4 Computational Specifics

4.4.1 Hamiltonian

A model hamiltonian of two harmonic oscillators with a quartic coupling term is used for the calculations

$$\hat{H} = \frac{p^2}{2m} + \frac{1}{2}m\omega^2(x^2 + y^2) + \lambda x^2 y^2, \tag{4.23}$$

where m is the mass, ω is the frequency of the modes, and λ is the coupling between the two modes. The mass is set equal to 1837 amu, and the frequencies of both modes are set to 2000 cm^{-1}. The coupling, *lambda* is varied between zero and one. When lambda is equal to zero (ie there is no coupling) the potential is spherically symmetric (see Figure 4.1). Trajectories on this potential are periodic over a short time period. As the coupling increases, the walls of the potential become steeper. The resulting trajectories become more chaotic, and the phase space integral is more difficult to converge.

4.4.2 The Wave Function and Overlaps

We choose $|\psi\rangle$ to be a product of two harmonic oscillator wave functions

$$|\psi\rangle = \sqrt{\frac{\omega}{\pi}} e^{-\frac{\omega}{2}(\mathbf{q}_0 - \mathbf{q}^0)^2}, \tag{4.24}$$

where the gaussians are centered about $\mathbf{q}^0$. The coherent states for use with the Herman-Kluk SCIVR are centered about the same point, $(\mathbf{q}^0, \mathbf{p}^0 = 0)$, and $\gamma = \omega$, which is a constant. Our overlaps are

$$\langle\psi|\mathbf{q}_t, \mathbf{p}_t, \gamma\rangle = e^{-\frac{\omega}{4}(\mathbf{q}_t - q^0)^2} e^{-\frac{1}{4\omega}\mathbf{p}_t^2} e^{-\frac{i}{2}\mathbf{p}_t(\mathbf{q}_t - \mathbf{q}^0)} \tag{4.25}$$

$$\langle \mathbf{q}_0, \mathbf{p}_0, \gamma | \psi \rangle = e^{-\frac{\omega}{4}(\mathbf{q}_0 - q^0)^2} e^{-\frac{1}{4\omega}\mathbf{p}_0^2} e^{\frac{i}{2}\mathbf{p}_0(\mathbf{q}_0 - \mathbf{q}^0)}. \tag{4.26}$$

For the time integration studies, recalling that γ is a function of time, and our overlaps take on a more complex form

$$\langle \psi | \mathbf{q}_t, \mathbf{p}_t, \gamma_t \rangle = \sqrt{\frac{\sqrt{\omega\gamma_t}}{\left(\frac{\omega+\gamma_t}{2}\right)}} e^{-\frac{1}{2}(\mathbf{q}_t - \mathbf{q}^0)\gamma_t(\gamma_t+\omega)^{-1}\omega(\mathbf{q}_t - \mathbf{q}^0)} \times e^{-\frac{1}{2}\mathbf{p}_t(\omega+\gamma_t)^{-1}\mathbf{p}_t} e^{-\frac{i}{2}\mathbf{p}_t(\mathbf{q}_t - \mathbf{q}^0)} \tag{4.27}$$

$$\langle \mathbf{q}_0, \mathbf{p}_0, \gamma_0 | \psi \rangle = \sqrt{\frac{\sqrt{\omega\gamma_0}}{\left(\frac{\omega+\gamma_0}{2}\right)}} e^{-\frac{1}{2}(\mathbf{q}_0 - \mathbf{q}^0)\gamma_0(\gamma_0+\omega)^{-1}\omega(\mathbf{q}_0 - \mathbf{q}^0)} \times e^{-\frac{1}{2}\mathbf{p}_0(\omega+\gamma_0)^{-1}\mathbf{p}_0} e^{\frac{i}{2}\mathbf{p}_0(\mathbf{q}_0 - \mathbf{q}^0)}. \tag{4.28}$$

4.4.3 HK-SCIVR

As we showed in a previous section, the HK-SCIVR expression of the spectrum of a molecule is

$$I(E) = \frac{1}{\pi(2\pi)^F} Re \int dt e^{iEt} \int d\mathbf{q}_0 \int d\mathbf{p}_0 C_t(\mathbf{q}_0, \mathbf{p}_0) e^{iS_t(\mathbf{q}_0, \mathbf{p}_0)} \times \langle \psi | \mathbf{q}_t, \mathbf{p}_t, \gamma \rangle \langle \mathbf{q}_0, \mathbf{p}_0, \gamma | \psi \rangle. \tag{4.29}$$

Evaluating the above equation is fairly straightforward. We use a gaussian weighting function and Monte Carlo sampling to evaluate the integrals over initial positions and momenta.

The reader should pay special attention to the calculation of the pre-exponential factor. When taking the square root of a complex number, one must be clear which branch is taken. For example, if the phase of $C_0(t)^2$ is just under 180 degrees, then the phase of the pre-exponential factor $(C_0(t))$ is just under 90 degrees (See Figure 4.2). However, when the phase of $C_0(t)^2$ is just over than 180 degrees, the phase of the pre-exponential factor is just over 270

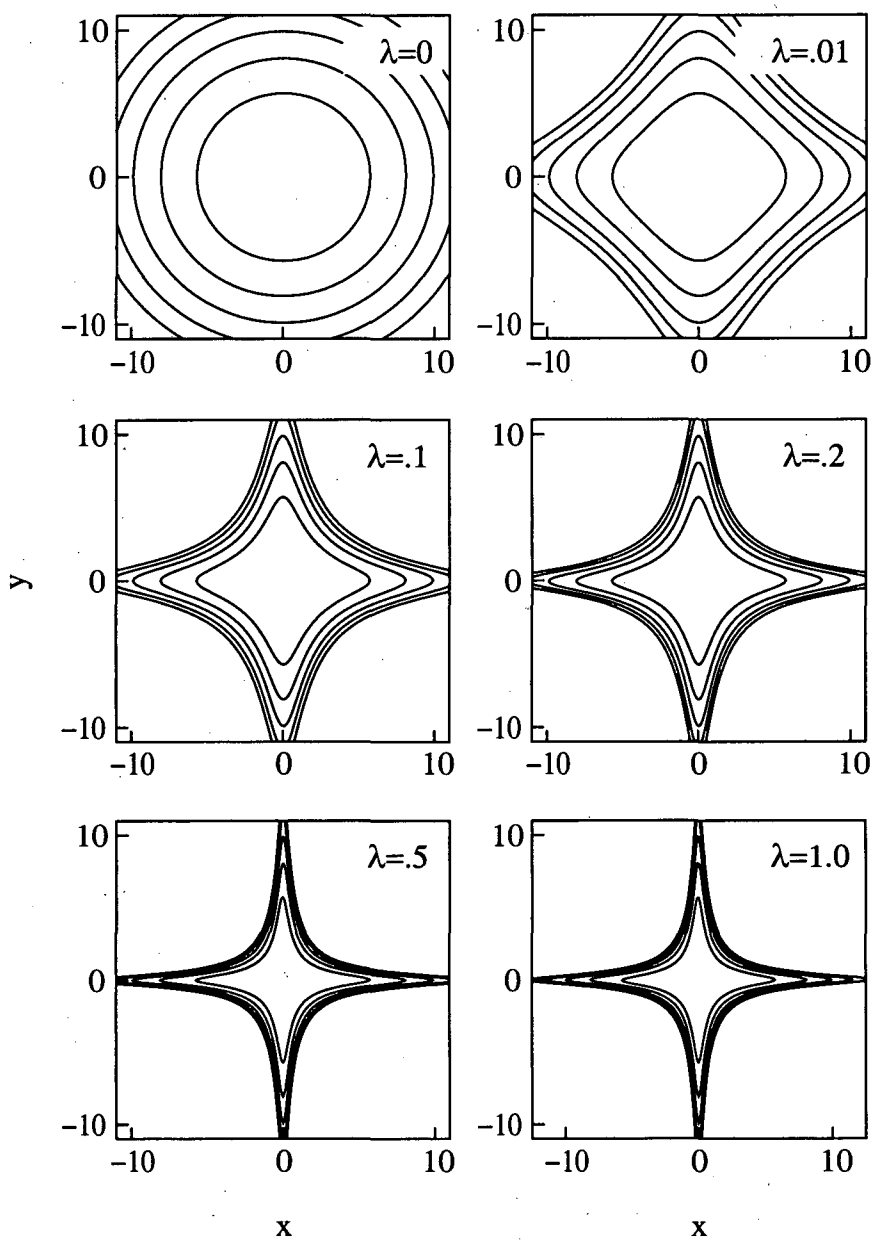

Figure 4.1: Contour lines for various values of λ, the coupling parameter. Contour lines are shown at intervals of 2.5 cm^{-1}, and E(0,0)=0 for all surfaces.

degrees. The pre-exponential factor is off by π. Thus we must keep track of the phase of the pre-exponential factor along the trajectory and use it to correct for the branch cuts

$$C_0(t) = C_0(t) * (-1)^v, \tag{4.30}$$

where v is the maslov index. The maslov index is an integer and is increased (decreased) by one every time the phase of the pre-exponential factor increases (decreases) by more than π. This necessitates a time step that is sufficiently small to capture all branch cuts.

In fact the pre-exponential factor is the most cumbersome part of the calculation. As the coupling between the two modes is increased, the trajectories become more chaotic, and a tiny change in initial position and momenta leads to a large deviation in the final phase point. This causes the magnitude of the pre-exponential factor to rise exponentially. Ultimately the chaotic nature of the trajectories causes the pre-exponential factor to grow so large that the Herman-Kluk SCIVR breaks down.

4.4.4 Time Averaging

The reader will recall our original expression for the time integrated SCIVR.

$$I(E) = \frac{1}{T\pi(2\pi)^F} Re \int d\mathbf{q}_0 \int d\mathbf{p}_0 \int_0^T dt \int_t^\infty dt' C_t(t') e^{iS_t(\mathbf{q}_0,\mathbf{p}_0) - S_{t'}(\mathbf{q}_0,\mathbf{p}_0)} \times \langle\psi|\mathbf{q}_{t'}, \mathbf{p}_{t'}, \gamma_{t'}\rangle\langle\mathbf{q}_t, \mathbf{p}_t, \gamma_t|\psi\rangle. \tag{4.31}$$

Unfortunately the calculation of the pre-exponential factor makes this method prohibitively expensive. For each trajectory the pre-exponential factor must be evaluated $n^2_{timesteps}$ and involves multiplying two 2n by 2n matrices. The maslov index must also be calculated, limiting the length of our time step.

After making the approximation to the monodromy matrix and our judicious

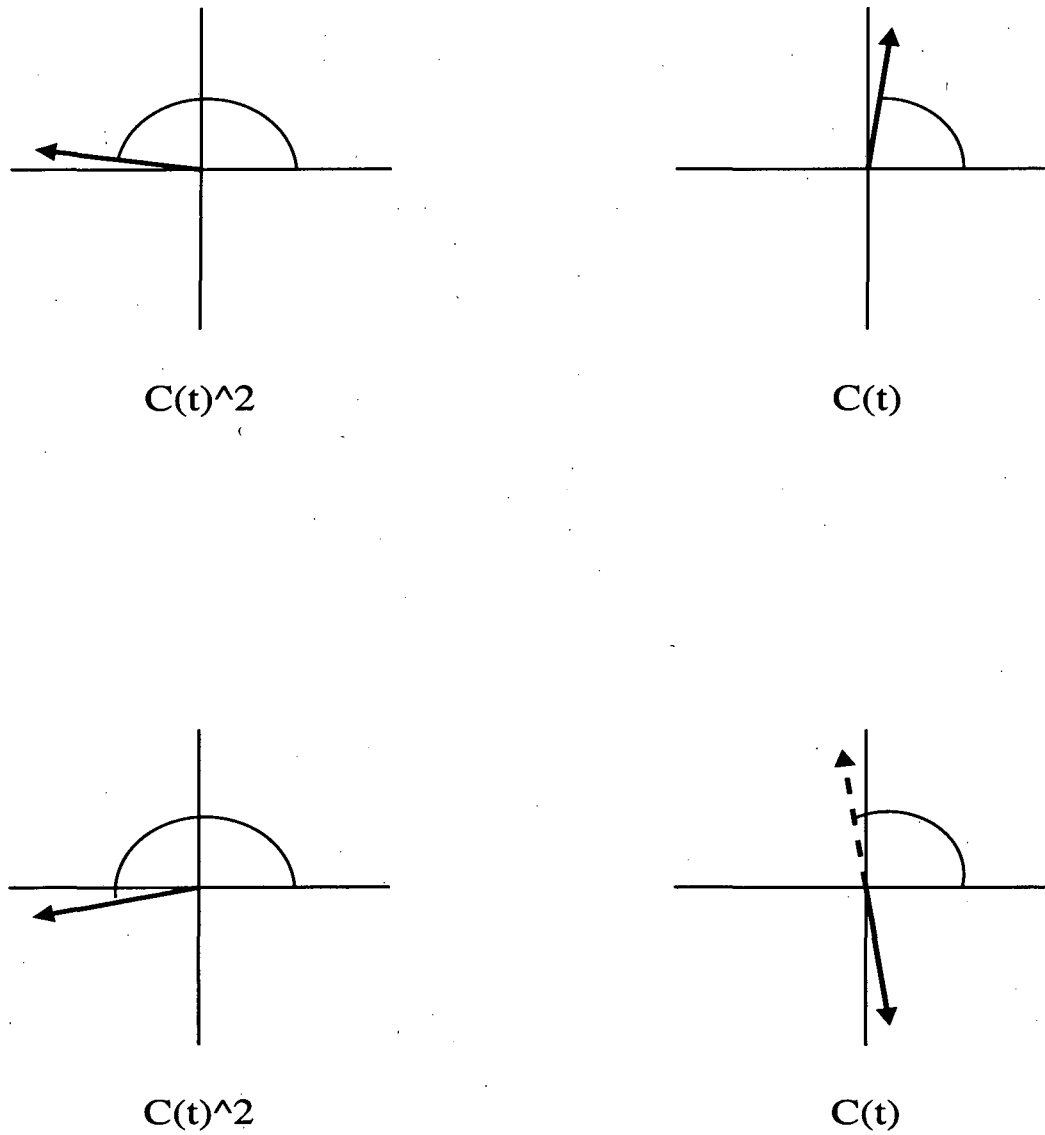

Figure 4.2: One must be careful when taking the square root of a complex number, as in the calculation of the pre-exponential factor. When the phase of $(C_0(t))^2$ is just under π, the phase of the pre-exponential factor $(C_0(t))$ is just under $\frac{\pi}{2}$. However, when the phase of $(C_0(t))^2$ is just over π, the phase of the pre-exponential factor $(C_0(t))$ is just over $\frac{3\pi}{2}$. This is off by a factor of π.

choice of γ

$$I(E) = \frac{1}{2\pi T(2\pi)^F} \int d\mathbf{q}_0 \int d\mathbf{p}_0 \left| \int_0^T e^{iEt} \langle \psi | \mathbf{q}_t, \mathbf{p}_t, \gamma_t \rangle e^{-i \int_0^t [p\dot{q} - \hat{H} - \sum_k \frac{1}{2}\omega_k(t')] dt'} \right|^2 \quad (4.32)$$

Notice that we no longer need to keep track of the maslov index because we are no longer taking the square root of a complex number. Also note that there is no obvious weighting function in the previous equation for use in the Monte Carlo sampling. In this case, we can perform the phase space integral using a flat distribution. However, others have shown that in the case of a harmonic oscillator system, sampling from a Husimi distribution[126] provides for faster convergence. In order to get the desired distribution, we divide and multiply equation 4.32 by $|\langle \mathbf{q}_0, \mathbf{p}_0, \gamma_0 | \psi \rangle|^2$.

$$\begin{aligned} I(E) = & \frac{1}{2\pi T(2\pi)^F} \int d\mathbf{q}_0 \int d\mathbf{q}_0 \, |\langle \mathbf{q}_0, \mathbf{p}_0, \gamma_0 | \psi \rangle\rangle|^2 \\ & \times \left| \int_0^T e^{iEt} \frac{\langle \psi | \mathbf{q}_t, \mathbf{p}_t, \gamma_t \rangle}{\langle \mathbf{q}_0, \mathbf{p}_0, \gamma_0 | \psi \rangle} e^{-i \int_0^t [p\dot{q} - \hat{H} - \sum_k \frac{1}{2}\omega_k(t')] dt'} \right|^2 . \end{aligned} \quad (4.33)$$

where the final term is the above expression is used as sampling function in the Monte Carlo evaluation of the phase space integral.

4.5 Results

We compare results using equations 4.29(HK-SCIVR) and 4.33(Time Averaging SCIVR). Calculations using time averaging without the approximation to the pre-exponential factor do not result in a decrease in the number of trajectories necessary for convergence. In addition, time integration SCIVR with a flat sampling function does yield a higher rate of convergence. However, using the Husimi distribution results in far superior convergence rates. We report the results of the Herman-Kluk SCIVR and the time averaged SCIVR with the adiabatic approximation to the pre-exponential factor.

We calculate the eigenvalues of the system by diagonalizing the hamiltonian and compare them with the results of the SCIVR methods. As seen in Figure

4.3, both the Herman-Kluk SCIVR and time integrated SCIVR produce peaks at the correct energies. With no coupling between the modes, we already see an significant increase on the rate of convergence by using a time averaged version of the SCIVR. While the Herman-Kluk SCIVR requires at least 1000 trajectories to converge, the time average method results in convergence after only five trajectories. Not only does the time averaged SCIVR converge in fewer trajectories, but the time spent evaluating the trajectory is decreased due to the elimination of the maslov index and the simplified expression for the pre-exponential factor.

As the coupling slowly increases, the Herman-Kluk SCIVR fails to converge at even low couplings. We use the Manolopoulus SCIVR[115] in an attempt to stretch the usefulness of the Herman-Kluk SCIVR, but the magnitude of the pre-exponential factor for many of the trajectories prohibits successful convergence. On the other hand, the time averaged SCIVR continues to perform magnificently. At a coupling of $\lambda = .01$, the agreement with the calculated eigenvalues is again quantitatively accurate. From this point on, we present only the time averaged results since conventional Herman-Kluk SCIVR fails.

At larger couplings, the time averaged method begins to show signs of weakness. At a coupling of $\lambda = .1$, we begin to see trajectories where some of the local frequencies are imaginary. As we questioned earlier, we need to identify what to do with these trajectories. Shown in Figure 4.6 are the results of two different approaches. The dashed line is the result of setting any imaginary frequencies equal to zero for the purpose of evaluating the spectrum. We stated earlier that this is equivalent to having no zero point energy contribution on top of a one-dimensional barrier. The solid line in Figure 4.5 is the result of rejecting the trajectories where a frequency meanders into the imaginary regime. We note both methods exhibit the same structural components. As we increase the coupling an increasing number of trajectories exhibit imaginary frequencies. See Table 4.1 for the percentages of such trajectories.

λ	% of trajectories with imaginary local frequencies
0	0%
.01	0%
.1	4%
.2	12%
.5	43%
1.0	61%

Table 4.1: Percent of trajectories with imaginary local frequencies for several values of the coupling parameter, λ.

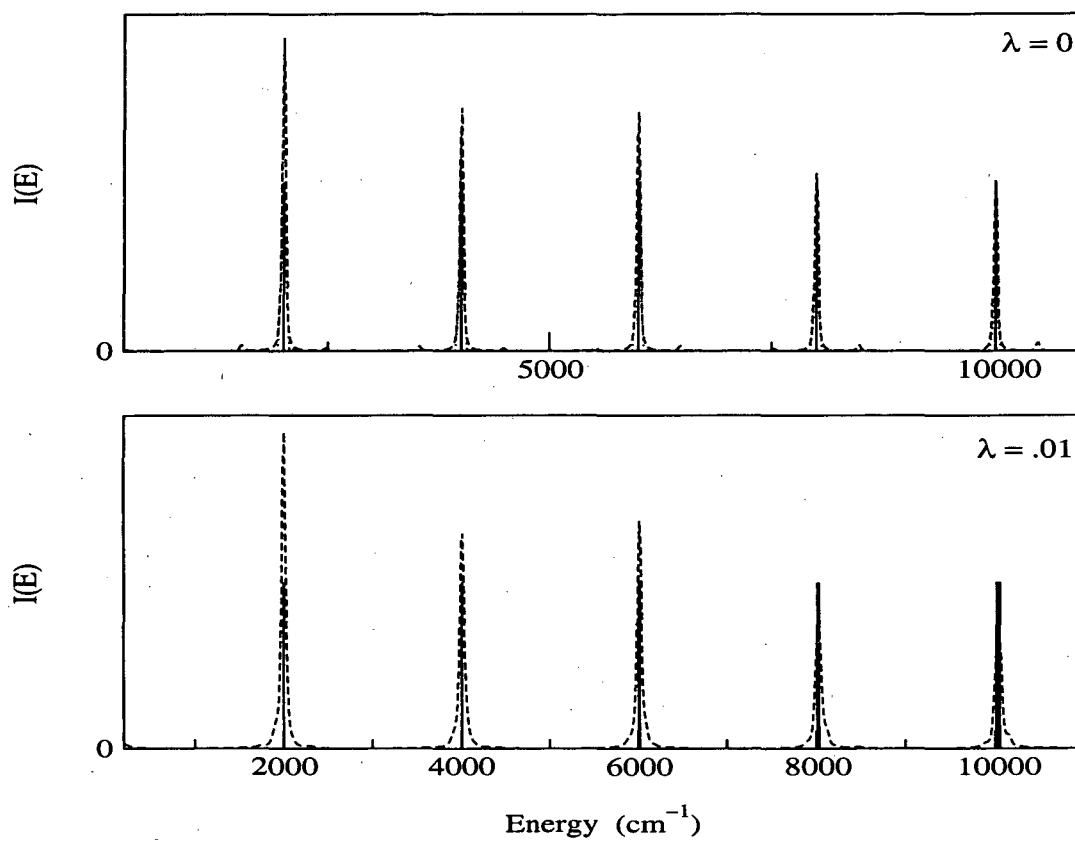

Figure 4.3: Spectrum of the model hamiltionian, $\hat{H} = \frac{p^2}{2} + \frac{1}{2}\omega^2(x^2 + y^2) + \lambda x^2 y^2$, where $\lambda = 0.0$ and .01. The solid verticle lines are the eigenvalues of the hamiltonian. The dashed line is the time averaged SCIVR result. The dotted line is the Herman-Kluk SCIVR result. Notice that the two SCIVR methods give the same results.

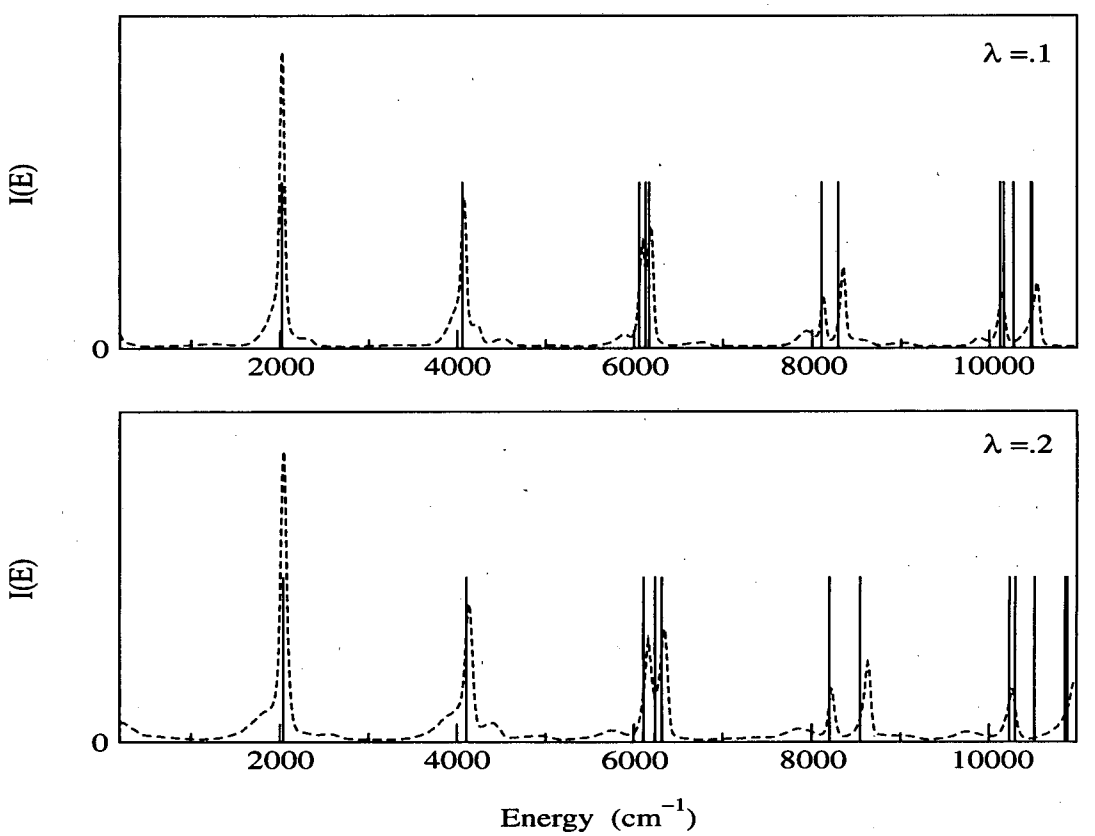

Figure 4.4: Spectrum of the model hamiltionian, $\hat{H} = \frac{p^2}{2} + \frac{1}{2}\omega^2(x^2+y^2) + \lambda x^2 y^2$, where $\lambda = .1$ and $.2$. The solid verticle lines are the eigenvalues of the hamiltonian. The dashed line is the time averaged SCIVR result.

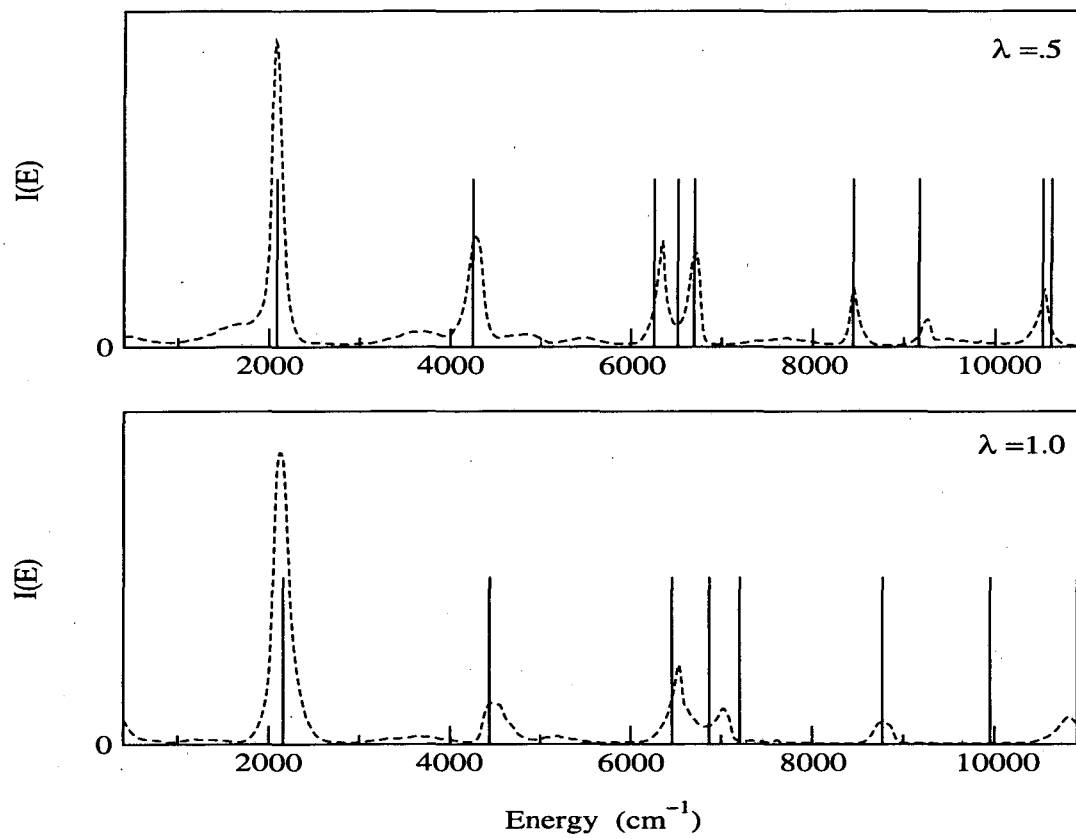

Figure 4.5: Spectrum of the model hamiltionian, $\hat{H} = \frac{p^2}{2} + \frac{1}{2}\omega^2(x^2 + y^2) + \lambda x^2 y^2$, where $\lambda = .5$ and 1.0. The solid verticle lines are the eigenvalues of the hamiltonian. The dashed line is the time averaged SCIVR result.

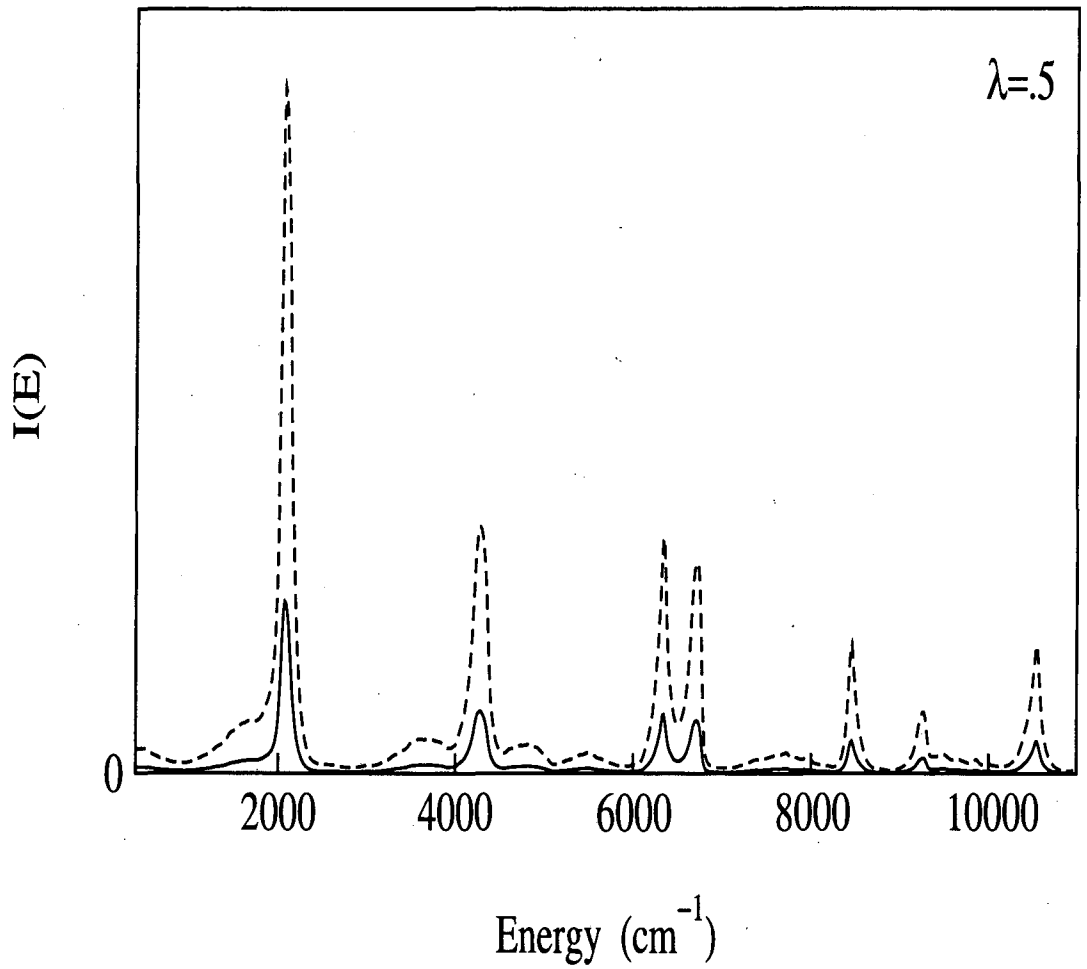

Figure 4.6: Spectrum for $\lambda = .5$. The solid line is the result of throwing out all trajectories that have imaginary local frequencies. The dashed line is the result of setting the zero point energy contribution to zero when those frequencies occur. Notice that both methods result in similar features.

For these larger couplings, time averaging provides good qualitative results. The reader will notice that not all peaks are present. This is due to our choice of $|\psi\rangle$, and should not cause concern. As the coupling is further increased, we see some spurious peaks in the spectra which do not disappear upon the addition of more trajectories. Most of the peaks are still centered about the eigenvalues, but a few have deviated slightly. The splittings in the spectra, while in generally good agreement, are overestimated to a small degree.

4.6 Conclusions

We have derived a modified version of the Herman-Kluk SCIVR. By inserting a time integral into the phase space integral, the rate of convergence using Monte Carlo techniques is greatly increased. Performing time integration (as well as using the adiabatic approximation for the monodromy matrix) extends the utility of the SCIVR to more chaotic systems where the HK-SCIVR can fail. In addition, the computational cost of each trajectory is significantly decreased. For zero coupling, we see a marked decrease in the number of trajectories necessary for convergence of the spectrum versus straightforward Herman-Kluk SCIVR. While the basic structure of the spectrum is reproduced, the splittings can be overestimated to a small degree in coupled systems when using the time averaged SCIVR. Whether or not this effect would be diminished or accentuated in a more complex chemical system remains to be seen. As the system becomes more chaotic, we are increasingly likely to encounter such imaginary local frequencies, which may or may not cause further deviation from the true spectra. Future studies may illuminate the matter.

Chapter 5

Summary and Conclusions

5.1 Summary

In this work, we have presented several semiclassical methods for obtaining the chemical properties of reactive and non-reactive systems. As mentioned in Chapter 1, quantum mechanical calculations become intractable as the number of dimensions in the chemical system of interest increases. Since we must deal with the computer resources available, semiclassical mechanics yield accurate results while diminishing the computational complexity of the problem. For several cases, we have shown the accuracy of various semiclassical approximations. While the agreement with experimental and quantum mechanical results is quite good, semiclassical techniques are approximations. Keeping this in mind, semiclassics still provides valuable insight into the dynamics of chemical systems.

In Chapter 2 we showed that Semiclassical Transition State Theory provides accurate rates for several reactions. SCTST improves on classical transition state theory by including a semiclassical description of the tunneling through the reaction barrier. The present formulation allows for an anharmonic parameterization of the potential energy surface and includes coupling between the reaction path and the orthogonal degrees of freedom. We saw that at higher temperatures agreement between SCTST, experiment, and quantum calculations was excellent.

Unfortunately, for reactions that involved hydrogen motion, the SCTST results underestimated the tunneling probabilities at lower temperatures. However, results for deuterium motion were in line with both experimental and quantum results. Thus, SCTST can be a valuable tool in the calculation of reaction rates where the reaction doesn't involve light atoms.

We reexamined the dissociation of triplet ketene into triplet methylene in Chapter 3. Experimental dissociation rates obtained by Moore and coworkers demonstrated a definite step structure[54,55]. Unfortunately, previous calculations performed by Gezelter and Miller failed to reproduce the step structure seen in experiments[63]. However, they were able to determine that using RRKM theory and a barrier frequency as high as 100 cm^{-1} did yield the desired structure. Recently a new, more complete potential surface has become available. We performed semiclassical calculations of the dissociation rate using the semiclassical perturbation and infinite order sudden approximations. Despite the inclusion of curvature coupling terms and an anharmonic potential, we were unable to reproduce the step structure with the improved potential surface. However, we did find that increasing the curvature coupling factors yielded the desired form. It is possible that the current surface underestimates the true curvature couplings. Another possible source of the structure is non-adiabatic intersystem crossings. This is currently under investigation in several research groups.

Finally we looked a new technique for smoothing the integrand of the Herman-Kluk Semiclassical Initial Value Representation. Recently there has been renewed interest in semiclassical initial value methods, where the propagator is represented by a phase space average. Unfortunately, the integrand is oscillatory which makes evaluating it difficult using Monte Carlo techniques. Many physical properties of molecules can be obtained using SCIVR methods. We chose to look specifically at the spectrum of a bound molecule. We proceeded by introducing identity in the form of a time integral into the equation for the spectrum. It was hoped that this would smooth the integrand, thus decreasing the number of trajectories

necessary for convergence. In fact we did see a dramatic decrease in the number of trajectories necessary for convergence. We also found that this allowed us to calculate properties for chaotic systems where traditional SCIVR fails. While time integration did yield noticeable benefits, the splittings in the spectrum were unfortunately overestimated as the chaotic nature of the system was increased. This is probably due to the approximation used for the pre-exponential factor that effectively adds the zero point energy. As the system became more chaotic, a greater number of trajectories experienced local imaginary frequencies, and the calculated spectrum deviates further from the true spectrum.

5.2 The Future of IVR Methods

Although significant progress has occurred recently in SCIVR methods, there are still difficulties to overcome. The forward-backward IVR method (mentioned briefly in Chapter 4), the Filinov transform, and adaptive sampling methods have proven useful. The ability of these methods to smooth the integrand is significant, allowing calculation of previously intractable systems. While these techniques are promising, they still fail in certain situations. Thus, we must continue to search out new smoothing methods.

Just recently, a new smoothing protocol has been developed by Wang, Manolopoulos and Miller[127]. Called the Modified Filinov, this method in effect shifts the Filinov transform. In the Filinov transform, we insert identity into the phase space integral in the form of a gaussian integral

$$1 = \left(\frac{\alpha}{\pi}\right)^{\frac{1}{2}} \int_{-\infty}^{\infty} dz e^{-\alpha(z_0-z)^2}. \tag{5.1}$$

Instead Wang has proposed inserting the following equation

$$1 = \left(\frac{\alpha}{\pi}\right)^{\frac{1}{2}} e^{\frac{-\beta^2}{4\alpha}} \int_{-\infty}^{\infty} dz e^{-\alpha(z_0-z)^2-\beta(z_0-z)}. \tag{5.2}$$

Similar to the derivation of the Filinov transform, Wang assumes that the system obeys linear dynamics. He then expands the integrand in a power series

around $z = z_0$. By assuming that β is purely imaginary, Wang is able to reduce the oscillatory nature of the integrand. Initial studies using this method are promising.

5.3 Conclusions

Although we would ideally be able to calculate all chemical properties quantum mechanically, this is impossible for large systems at this point in time due to hardware and theoretical constraints. As computers become more powerful, previously intractable calculations will become possible. Until then we must suffice to use approximate methods. However, our current efforts are not in vain. The results of many such techniques are in qualitative agreement with quantum mechanical calculations. Today, semiclassical mechanics offers a feasible method for calculating quantum mechanical properties.

References

[1] E. Wigner, *Trans. Faraday Soc.* , **34**, 29 (1938).

[2] H. Eyring, *Trans. Faraday Soc.* , **34**, 41 (1938).

[3] S. Glasstone, K. J. Laidler and H. Eyring, *Theory of Rate Processes*, McGraw-Hill, New York (1941).

[4] H. S. Johnston, *Gas Phase Reaction Rate Theory*, Ronald Press, New York (1966).

[5] D. L. Bunker, *Theory of Gas Phase Reaction Rates*, Pergamon Press, Oxford (1966).

[6] K. J. Laidler, *Theories of Chemical Reaction Rates*, McGraw-Hill, New York (1969).

[7] R. E. Weston and H. A. Schwatrz, *Chemical Kinetics*, Prentice-Hall, Englewood Cliffs (1972).

[8] I. W. M. Smith, *Kinetics and Dynamics of Elementary Gas Reactions*, Butterworths, London (1980).

[9] G. C. Shatz and A. Kuppermann, *J. Chem. Phys.* , **65**, 4668 (1976).

[10] J. C. Keck, *Adv. Chem. Phys.* , **13**, 85 (1967).

[11] R. B. Walker and J. C. Light, *Annu. Rev. Phys. Chem.* , **31**, 401 (1980).

[12] D. G. Truhlar and B. C. Garrett, *Annu. Chem. Rev.* , **13**, 440 (1980).

[13] P. Pechukas, *Annu. Rev. Phys. Chem.* , **32**, 159 (1981).

[14] W. L. Hase, *Annu. Chem. Rev.* , **16**, 258 (1983).

[15] W. H. Miller, R. Hernandez, N. C. Handy, D. Jayatilaka and A. Willetts, *Chem. Phys. Lett.* , **172**, 62 (1990).

[16] M. J. Cohen, N. C. Handy, R. Hernandez and W. H. Miller, *Chem. Phys. Lett.* , **192**, 407 (1992).

[17] R. Hernandez and W. H. Miller, *Chem. Phys. Lett.* , **214**, 129 (1993).

[18] M. J. Cohen, A. Willetts, and N. C. Handy, *Chem. Phys. Lett.* , **99**, 5885 (1993).

[19] R. Hernandez and W. H. Miller, *J. Chem. Phys.* , **101**, 9534 (1994).

[20] W. H. Miller, *J. Chem. Phys.* , **61**, 4301 (1974).

[21] W. H. Miller, *J. Chem. Phys.* , **63**, 1166 (1975).

[22] S. Chapman, B. C. Garrett, and W. H. Miller, *J. Chem. Phys.* , **63**, 2710 (1975).

[23] D. Papousek and M. R. Aliev, *Molecular Vibrational-Rotational Spectra*, Elsevier, Amsterdam, 1982.

[24] I. M. Mills, *Molecular Spectroscopy: Modern Research*, Academic Press, New York, 1972.

[25] J. Bron and M. Wolfsberg, *J. Chem. Phys.* , **57**, 2862 (1971).

[26] W. H. Green, D. Jayatilaka, A. Willetts, R. D. Amos, and N. C. Handy, *J. Chem. Phys.* , **93**, 4965 (1990).

[27] I. C. Percival, *Adv. Chem. Phys.* , **36**, 1 (1977).

[28] W. H. Miller, *Science* , **233**, 171 (1977).

[29] D. E. Reisner , R. W. Field, J. L. Kinsey and H. L. Dai, *J. Chem. Phys.* , **80**, 5968 (1984).

[30] W. H. Miller, *Faraday Disc. Chem. Soc.* , **62**, 40 (1977).

[31] L. D. Landau and E. M. Lifshitz, *Quantum Mechanics*, Pergamon Press, Oxford, 1965.

[32] R. Hernandez, Ph.D. Thesis, University of California at Berkeley, 1994.

[33] H. S. Johnston, *Gas Phase Reaction Rate Theory*, Ronald Press Co., New York, 1966.

[34] N. Froman and P. O. Froman, *JWKB Approximation*, North-Holland, Amsterdam, 1982.

[35] A. D. Isaacson, *J. Phys. Chem.* , **96**, 531 (1992).

[36] S. P. Walch and T. H. Dunning Jr., *J. Chem. Phys.* , **72**, 1303 (1980).

[37] A. Willetts, J. F. Gaw, W. H. Green, and N. G. Handy, SPECTRO: Theoretical Spectroscopy Package, Cambridge (1990).

[38] G. Herzberg, *Spectra of Diatomic Molecules*, 2nd edition, Van Nostrand, Reinhold (1950).

[39] A. R. Ravishankara, J. M. Nicovich, R. L. Thompson, and F. P. Tully, *J. Chem. Phys.* , **85**, 2498 (1981).

[40] S. S. Kumaran, K. P. Lim, and J. V. Michael, *J. Chem. Phys.* , **101**, 9487 (1994).

[41] M. Alagia, N. Balucani, L. Cartechini, P. Casavecchia, E. H. vanKleef, G. G. Volpi, F. J. Aoiz, L. Banares, D. W. Schwenke, T. C. Alloson, S. L. Mielke, and D. G. Truhlar, *Science* , **273**, 1519 (1996).

[42] H. Wang, W. H. Thompson, and W. H. Miller, *J. Chem. Phys.* , **107**, 7194 (1997).

[43] T. C. Allison, G. C. Lynch, D. G. Truhlar, and M. S. Gordon, *J. Phys. Chem.* , **100**, 13575 (1996).

[44] S. L. Mielke, T. C. Allison, D. G. Truhlar, and D. W. Schwenke, *J. Phys. Chem.* , **100**, 13588 (1996).

[45] I. C. Chen and C. B. Moore, *J. Chem. Phys.* , **94**, 263 (1990).

[46] I. C. Chen and C. B. Moore, *J. Chem. Phys.* , **94**, 269 (1990).

[47] S. K. Kim, Y. S. Choi, C. D. Pibel, Q. Zheng, and C. B. Moore, *J. Chem. Phys.* , **94**, 1954 (1991).

[48] C. C. Pan, C. C. Chou, C. H. Lu, Y. Tai, and K. C. Lin, *J. Chem. Phys.* , **107**, 3797 (1997).

[49] C. G. Morgan, M. Drabbels, and A. M. Wodtke, *J. Chem. Phys.* , **105**, 4550 (1996).

[50] M. Castillejo, M. Martín, R. deNalda, and J. Salís, *Chem. Phys. Lett.* , **268**, 465 (1997).

[51] M. Castillejo, S. Couris, E. Lane, M. Martin, and J. Ruiz, *Chem. Phys.* , **232**, 353 (1998).

[52] E. R. Lovejoy, R. A. Alvarez, and C. B. Moore, *J. Chem. Phys.* , **95**, 4081 (1991).

[53] E. R. Lovejoy and C. B. Moore, *J. Chem. Phys.* , **98**, 7846 (1993).

[54] S. K. Kim, E. R. Lovejoy, and C. B. Moore, *J. Chem. Phys.* , **102**, 3202 (1995).

[55] E. R. Lovejoy, S. K. Kim, and C. B. Moore, *Science* , **256**, 1541 (1992).

[56] W. H. Green, A. J. Mahoney, Q. Zhang, and C. B. Moore, *J. Chem. Phys.* , **94**, (1991).

[57] I. Garcia-Moreno, E. R. Lovejoy, and C. B. Moore, *J. Chem. Phys.* , **100**, 8890 (1994).

[58] I. Garcia-Moreno, E. R. Lovejoy, and C. B. Moore, *J. Chem. Phys.* , **100**, 8902 (1994).

[59] A. Mellinger, M. V. Ashikhmin, and C. B. Moore, *J. Chem. Phys.* , **108**, 8944 (1998).

[60] E. A. Wade, A. Mellinger, M. A. Hall, and C. B. Moore, *J. Phys. Chem. A* , **101**, 6568 (1997).

[61] A. J. Rasmussen, K. E. Gates, and S. C. Smith, *J. Chem. Phys.* , **110**, 1354 (1999).

[62] S. J. Klippenstein, A. L. West, and W. D. Allen, *J. Chem. Phys.* , **105**, 118 (1996).

[63] J. D. Gezelter and W. H. Miller, *J. Chem. Phys.* , **104**, 3546 (1996).

[64] J. D. Gezelter and W. H. Miller, *J. Chem. Phys.* , **103**, 7868 (1995).

[65] A. L. East, W. D. Allen, and S. J. Klippenstein, *J. Chem. Phys.* , **102**, 8506 (1995).

[66] P. G. Szalay, A. G. Császár, and L. Nemes, *J. Chem. Phys.* , **105**, 1034 (1996).

[67] Q. Cui and K. Morokuma, *J. Chem. Phys.* , **107**, 4951 (1997).

[68] J. Troe and C. B. Moore (private communication).

[69] I. C. Chen and C. B. Moore, *J. Phys. Chem.* , **94**, 263 (1990).

[70] S. J. Klippenstein, A. L. East, and W. D. Allen, *J. Chem. Phys.* , **105**, 118 (1996).

[71] R. A. King, W. D. Allen, B. Ma, and H. F. Schaeffer III, unpublished.

[72] D. G. Truhlar and A. Kuppermann, *J. Chem. Phys.* , **56**, 2232 (1972).

[73] T. Seideman and W. H. Miller, *J. Chem. Phys.* , **97**, 2499 (1992).

[74] W. H. Miller and S. Shi, *J. Chem. Phys.* , **75**, 2258 (1981).

[75] W. H. Miller, N. C. Handy, and J. E. Adams, *J. Chem. Phys.* , **72**, 99 (1980).

[76] J. M. Bowman, *J. Phys. Chem.* , **95**, 4960 (1991).

[77] S. Takada, A. Ohsaki, and H. Nakamura, *J. Chem. Phys.* , **96**, 339 (1992).

[78] S. M. Auerbach and W. H. Miller, *J. Chem. Phys.* , **100**, 1103 (1994).

[79] W. H. Miller, *J. Chem. Phys.* , **53**, 3578 (1970).

[80] W. H. Miller and T. F. George, *J. Chem. Phys.* , **56**, 5668 (1972).

[81] M. F. Herman and E. Kluk, *Chem. Phys.* , **91**, 27 (1984).

[82] E. Kluk, M. F. Herman, and H. L. Davis, *J. Chem. Phys.* , **84**, 326 (1986).

[83] M. F. Herman, *Chem. Phys. Lett.* , **275**, 445 (1997).

[84] B. E. Guerin and M. F. Herman, *Chem. Phys. Lett.* , **286**, 361 (1998).

[85] K. G. Kay, *J. Chem. Phys.* , **100**, 4377 (1994).

[86] K. G. Kay, *J. Chem. Phys.* , **100**, 4432 (1994).

[87] K. G. Kay, *J. Chem. Phys.* , **107**, 2313 (1997).

[88] A. R. Walton and D. E. Manolopoulos, *Chem. Phys. Lett.* , **244**, 448 (1995).

[89] M. L. Brewer, J. S. Hume and D. E. Manolopoulos, *J. Chem. Phys.* , **106**, 4832 (1996).

[90] G. Stock and M. Thoss, *Phys. Rev. Lett.* , **78**, 578 (1997).

[91] J. L. McWhirter, *J. Chem. Phys.* , **112**, 7891 (2000).

[92] S. Garashchuk and D. J. Tannor, *Chem. Phys. Lett.* , **262**, 477 (1996).

[93] F. Grossman, *Chem. Phys. Lett.* , **262**, 470 (1996).

[94] G. Campolieti and P. Brummer, *Phys. Rev. A* , **50**, 997 (1994).

[95] D. Provost and P. Brummer, *Phys. Rev. Lett.* , **74**, 250 (1995).

[96] E. J. Heller, *J. Chem. Phys.* , **94**, 2723 (1991).

[97] E. J. Heller, *J. Chem. Phys.* , **94**, 9431 (1991).

[98] M. A. Sepulveda, S Tomsoivc and E. J. Heller, *Phys. Rev. Lett.* , **69**, 402 (1992).

[99] N. T. Maitra and E. J. Heller, *Phys. Rev. Lett.* , **78**, 3035 (1997).

[100] W. H. Miller, *Adv. Chem. Phys.* , **25**, 69 (1974).

[101] W. H. Miller, *J. Chem. Phys.* , **95**, 9428 (1991).

[102] S. Keshavamurthy and W. H. Miller, *Chem. Phys. Lett.* , **218**, 189 (1994).

[103] B. W. Spath and W. H. Miller, *J. Chem. Phys.* , **104**, 95 (1996).

[104] X. Sun and W. H. Miller, *J. Chem. Phys.* , **106**, 6346 (1997).

[105] W. H. Miller, *Faraday Disc. Chem. Soc.* , **110**, 1 (1998).

[106] D. E. Skinner and W. H. Miller, *Chem. Phys. Lett.* , **300**, 20 (1998).

[107] V. S. Batista and W. H. Miller, *J. Chem. Phys.* , **108**, 498 (1998).

[108] H. Wang, X. Sun and W. H. Miller, *J. Chem. Phys.* , **108**, 9726 (1998).

[109] X. Sun, H. Wang and W. H. Miller, *J. Chem. Phys.* , **109**, 4190 (1998).

[110] X. Sun, H. Wang and W. H. Miller, *J. Chem. Phys.* , **109**, 7064 (1998).

[111] V. S. Batista, M. T. Zanni, B. Breenblatt, D. M. Neumark and W. H. Miller, *J. Chem. Phys.* , **110**, 3736 (1999).

[112] V. Guallar, V. S. Batista and W. H. Miller, *J. Chem. Phys.* , **110**, 9922 (1999).

[113] H. Wang, M. Thoss, K. L. Sorge, R. Gelebert, X. Gimenez, and W. H. Miller, in press.

[114] K. G. Kay, *J. Chem. Phys.* , **101**, 2250 (1994).

[115] A. R. Walton and D. E. Manolopoulos, *Molec. Phys.* , **87**, 961 (1996).

[116] J. Cao and G. A. Voth, *J. Chem. Phys.* , **104**, 273 (1996).

[117] X. Sun and W. H. Miller, *J. Chem. Phys.* , **108**, 8870 (1998).

[118] G. Campolieti and P. Brummer, *J. Chem. Phys.* , **109**, 2999 (1998).

[119] K. Thompson and N. Makri, *Chem. Phys. Lett.* , **291**, 101 (1998).

[120] K. Thompson and N. Makri, *J. Chem. Phys.* , **110**, 1343 (1999).

[121] X. Sun and W. H. Miller, *J. Chem. Phys.* , **110**, 6635 (1999).

[122] D. E. Skinner and W. H. Miller, *J. Chem. Phys.* , **111**, 10787 (2000).

[123] H. Wang, M. Thoss, and W. H. Miller, *J. Chem. Phys.* , **112**, 47 (2000).

[124] Y. Elran and K. G. Kay, *J. Chem. Phys.* , **110**, 3653 (1999).

[125] Y. Elran and K. G. Kay, *J. Chem. Phys.* , **110**, 8912 (1999).

[126] K. Husimi, *Proc. Phys. Math. Soc. Japan* , **22**, 264 (1940).

[127] H. Wang, W. H. Miller, and D. E. Manolopoulos (private communication).

Ernest Orlando Lawrence Berkeley National Laboratory
One Cyclotron Road | Berkeley, California 94720

Prepared for the U.S. Department of Energy under Contract No. DE-AC03-76SF00098